Next Generation Very Large Array Memo #106

# ngVLA Imaging Science Performance Reference Document

Viviana Rosero (NRAO), Chris Carilli (NRAO)

November 28, 2022

## Contents

**1 Introduction** **3**
1.1 Purpose . . . 3
1.2 Abbreviations & Acronyms . . . 3
1.3 Overview: The ngVLA Configuration . . . 3

**2 Performance of the ngVLA** **7**
2.1 Taperability . . . 7
2.2 Subarrays . . . 9
2.3 Simulated Resolution and PSF . . . 11
2.4 Beam Sculpting . . . 12
2.4.1 Combination of Imaging Parameters . . . 13
2.4.2 Selection of Subarrays . . . 15
2.5 Sensitivity of the ngVLA . . . 18
2.5.1 Continuum Point Source Sensitivity . . . 18
2.5.2 Line Sensitivity . . . 21
2.5.3 Continuum Brightness Sensitivity . . . 23
2.5.4 Line Brightness Sensitivity . . . 25

**3 Image Fidelity** **27**
3.1 KSG 1: Protoplanetary Disks . . . 27
3.1.1 Model and Simulations . . . 27
3.1.2 Determination of Imaging Parameters . . . 29
3.1.3 Images with the Desired Resolution . . . 30
3.1.4 Results . . . 30
3.2 KSG 3 (NGA8): Imaging Molecular Gas in Nearby Galaxies . . . 34
3.2.1 Model and Simulations . . . 34
3.2.2 Imaging . . . 36
3.2.3 Results . . . 36

3.2.4 Comparison Study of image Fidelity using ngVLA RevC and RevD . . . 39

**4 High Dynamic Range Imaging** **40**
4.1 Model, Configuration, and Processing . . . 40
4.2 Results . . . 41
4.3 Summary . . . 43

**5 On the Fly Mapping** **45**

# List of Figures

1 The ngVLA Configuration (RevD) . . . 5
2 ngVLA naturally weigthed PSF (RevD) . . . 7
3 Taperability Curve for the ngVLA Main+LBA components . . . 8
4 Taperability Curves for the ngVLA Components and Selected Subarrays . . . 10
5 PSF combination examples of robust and uv-taper values producing the same angular resolution. . . . 11
6 Change of sensitivity with Briggs robust at the same angular resolution . . . 12
7 Simulated 30 GHz PSFs for the ngVLA Reference Array . . . 13
8 PSF level at one FWHM (i.e., metric 2b) . . . 14
9 Results of metric 2b for a resulting angular resolution of 5 mas . 15
10 PSF profiles of the naturally weighted synthesized beam for subarrays that includes the Spiral plus different fractions of the Core. 16
11 Efficiency curves for selected resolutions and subarrays . . . 17
12 Continuum Point Source Sensitivity of the ngVLA Main+LBA Components . . . 19
13 Continuum Sensitivity Over a Range of Resolutions for the ngVLA Main+LBA Components . . . 20
14 Line source sensitivity of the ngVLA Main+LBA subarray . . . 21
15 Line sensitivity over a range of resolutions for the ngVLA Main+LBA subarray . . . 22
16 Continuum brightness sensitivity of the ngVLA Main+LBA subarray . . . 23
17 Continuum brightness sensitivity over a range of resolutions for the ngVLA Main+LBA subarray . . . 24
18 Line brightness sensitivity of the ngVLA for the Main+LBA subarray . . . 25
19 Line brightness sensitivity over a range of resolutions for the ngVLA Main+LBA subarray . . . 26
20 Synthetic model image for a planetary disk at 3 mm from KSG 1 28
21 Robust as a function of uv-taper for KSG 1 . . . 29
22 Fidelity vs robust . . . 31

23 Fidelity example R= −1.6 . . . . . . . . . . . . . . . . . . . . . . 32
24 Residuals (noise-free) R= −1.6 . . . . . . . . . . . . . . . . . . . 33
25 Residuals (noisy) R= −1.6 . . . . . . . . . . . . . . . . . . . . . . 33
26 Model image for KSG 3 NGA8 . . . . . . . . . . . . . . . . . . . . 35
27 Feathered Image . . . . . . . . . . . . . . . . . . . . . . . . . . . 37
28 Image of the convolved model subtracted from the final image . . 38
29 Image of the relative residuals . . . . . . . . . . . . . . . . . . . . 38
30 Median fraction of spatially integrated flux density recovered as a function of aperture diameter . . . . . . . . . . . . . . . . . . . 39
31 Simulated images of Cygnus A . . . . . . . . . . . . . . . . . . . . 42
32 Fidelity image of Cygnus A . . . . . . . . . . . . . . . . . . . . . . 43
33 Images of the synthesized beam . . . . . . . . . . . . . . . . . . . 44

# 1 Introduction

## 1.1 Purpose

To have an understanding of the performance of the ngVLA in terms of the sensitivity, and how it changes with resolution and frequency. Additionally, developing studies of beam sculpting and imaging fidelity for selected key science goals.

## 1.2 Abbreviations & Acronyms

KSG ......... Key Science Goals
LAS ......... Largest Angular Scale
LBA ......... Long Baseline Array
MFS ......... Multi-Frequency Synthesis
ngVLA ......... next generation Very Large Array
SBA ......... Short Baseline Array
PSF ......... Point Spread Function

## 1.3 Overview: The ngVLA Configuration

The ngVLA antenna locations have been chosen to accommodate a wide variety of scientific observations, aiming to deliver high sensitivity over a wide range of resolutions with a non-reconfigurable array. The key science requirements are the main drivers of the array design. The science requirements are a result of the science use cases identified by the ngVLA Science Working Groups and the ngVLA Science Advisory Council (see ngVLA Science Requirements document [13]). The five key science goals (KSGs) of the ngVLA are the following:

- **KSG1** – Unveiling the Formation of Solar System Analogues

- **KSG2** – Probing the Initial Conditions for Planetary Systems and Life with Astrochemistry
- **KSG3** – Charting the Assembly, Structure, and Evolution of Galaxies from the First Billion Years to the Present
- **KSG4** – Using Pulsars in the Galactic Center to Make a Fundamental Test of Gravity
- **KSG5** – Understanding the Formation and Evolution of Stellar and Supermassive Black Holes in the Era of Multi-Messenger Astronomy

The ngVLA configuration (RevD – ngVLA memo #92 [9] ; see Figure 1) includes three fundamental components:

- A Main Array (MA) of 214 x 18 m antennas
- A Long Baseline Array (LBA) of 30 x 18 m antennas
- A Short Baseline Array (SBA) of 19 x 6 m antennas

Depending on the science requirements, the ngVLA can in principle operate with combinations of different subarrays (see Table 1 for a list of selected subarrays). The Main array can be characterized by three sub-components or scales: the Core, the Spiral and the Mid-baselines. The *Core* consists of 114 18 m antennas in a dense semi-random distribution within a region of $\sim$4 km diameter, providing high surface brightness sensitivity at $\sim$1,000 mas resolution needed for KSG 3. The five-armed *Spiral* is composed of 54 18 m antennas, extending from the edge of the Core out to $\sim$39 km baselines within the Plains of San Agustin, and capable of high-fidelity imaging at $\sim$100 mas scales important for KSGs 2 and 3. The *Mid* sub-component consists of 46 18 m antennas, distributed in a roughly longer multi-arm spiral pattern, expanding into parts of Texas, Arizona, and Northern Mexico, providing baselines for imaging at $\sim$10 mas required for KSGs 1 and 2.

The Main array will be augmented by a very compact array of smaller antennas (SBA) which will provide sensitivity on larger angular scales, and four antennas of the main array will be equipped to measure total power in order to fill in the center of the (u,v)-plane.

Additionally, the Long Baseline Array (LBA) consists of 10 continental-scale stations of 3 18 m antennas each that will provide baselines for achieving resolutions of $\sim$0.1 mas needed for KSGs 4 and 5. Long baseline stations are located in Hawaii, Washington, California, Iowa, West Virginia, New Hampshire, Puerto Rico, the US. Virgin Islands, and Canada.

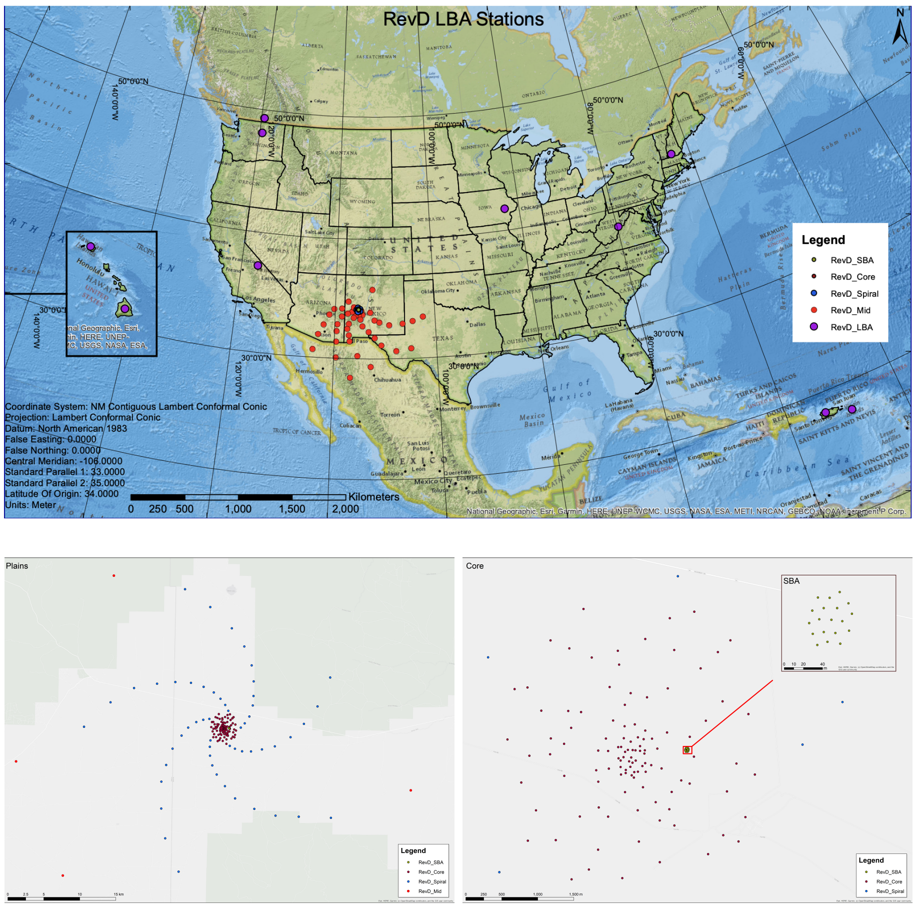


Figure 1: (*Top*) ngVLA Main array (i.e., Spiral and Core sub-components represented by the blue dots and Mid sub-component represented by the red dots) and LBA stations (represented by the purple dots) consisting of 244 18 m antennas total. (*Bottom left*) Spiral and Core sub-components represented by the blue and small red dots, respectively. (*Bottom right*) Core subcomponent and zoom-in of the SBA.

Table 1: Selected ngVLA components/subarrays, their naturally-weighted resolution ($\theta_{Nat}$) and LAS

| | | | | 2.4 GHz | | 8 GHz | | 16 GHz | | 27 GHz | | 41 GHz | | 93 GHz | |
|---|---|---|---|---|---|---|---|---|---|---|---|---|---|---|---|
| Component/ Subarray | # Ant. | $B_{max}$ [km] | $B_{min}$ [m] | $\theta_{Nat}$ [mas] | LAS [arcsec] | $\theta_{Nat}$ [mas] | LAS [arcsec] | $\theta_{Nat}$ [mas] | LAS [arcsec] | $\theta_{Nat}$ [mas] | LAS [arcsec] | $\theta_{Nat}$ [mas] | LAS [arcsec] | $\theta_{Nat}$ [mas] | LAS [arcsec] |
| Main+LBA | 244 | 8857.2 | 36.4 | 11.71 | 354.85 | 3.51 | 106.46 | 1.76 | 53.23 | 1.04 | 31.54 | 0.69 | 20.77 | 0.30 | 9.16 |
| LBA | 30 | 8857.2 | 36.4 | 3.77 | 354.85 | 1.13 | 106.46 | 0.57 | 53.23 | 0.34 | 31.54 | 0.22 | 20.77 | 0.10 | 9.16 |
| Main | 214 | 1068.3 | 39.4 | 81.83 | 327.83 | 24.55 | 98.35 | 12.27 | 49.18 | 7.27 | 29.14 | 4.79 | 19.19 | 2.11 | 8.46 |
| Mid | 46 | 1068.3 | 17147.1 | 36.43 | 0.75 | 10.93 | 0.23 | 5.46 | 0.11 | 3.24 | 0.07 | 2.13 | 0.04 | 0.94 | 0.02 |
| Spiral+Core | 168 | 39.3 | 39.4 | 1846.24 | 327.83 | 553.87 | 98.35 | 276.94 | 49.18 | 164.11 | 29.14 | 108.07 | 19.19 | 47.64 | 8.46 |
| Core | 114 | 4.3 | 39.4 | 9069.77 | 327.83 | 2720.93 | 98.35 | 1360.47 | 49.18 | 806.20 | 29.14 | 530.91 | 19.19 | 234.06 | 8.46 |
| Spiral | 54 | 39.3 | 811.0 | 951.85 | 15.93 | 285.56 | 4.78 | 142.78 | 2.39 | 84.61 | 1.42 | 55.72 | 0.93 | 24.56 | 0.41 |

Note: $B_{max}$ and $B_{min}$ are the *unprojected* maximum and minimum baseline lengths, respectively. The naturally-weighted resolution is defined as $\theta_{Nat} \approx \lambda/B_{max}$ [rad].
The reported LAS is based on the minimum baseline resolution divided by two, the same approach used for estimating the LAS of the VLA. Thus, minimum baseline resolution$\sim 6.2 \times 10^4/(\nu[GHz] * B_{min}[m])$[arcsec]. Detailed simulations are needed to find more accurate results for the ngVLA.

# 2 Performance of the ngVLA

The centrally condensed antenna distribution of the ngVLA leads to a naturally weighted beam that is not well characterized by a Gaussian function (see e.g., ngVLA memo #12 [3] and ngVLA memo #41 [6]). Specifically, the long baselines produce a very narrow peak in the point spread function (PSF) and the core contributes a broad skirt (as seen in Figure 2).

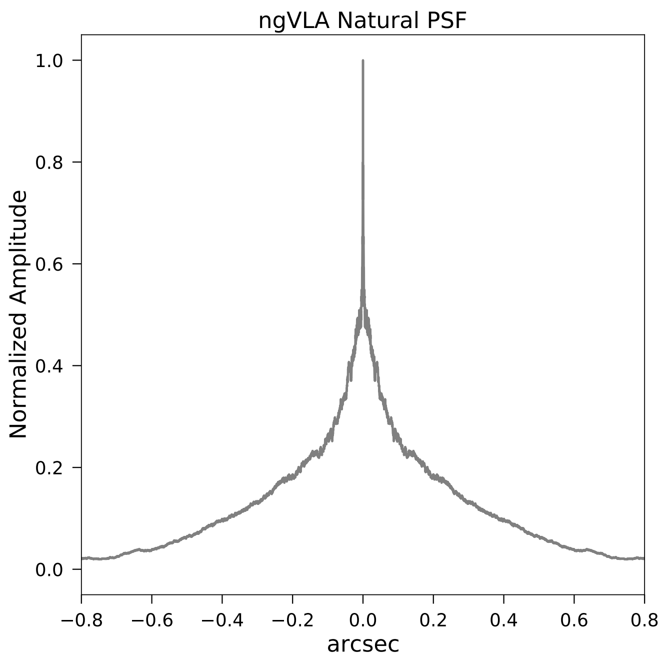


Figure 2: 1D East-West cuts through ngVLA natural PSF for RevD

Specific science applications may need to adjust the uv-weighting and other image parameters to 'sculpt' a synthesized beam that is suitable for the particular science goal being considered and also to change the resolution. In ngVLA memo #55 [17], V. Rosero performed a taperability study as a metric to compare different subarrays from the ngVLA configuration and their performance at different resolutions as measured in terms of their relative sensitivity (see Section 2.1).

## 2.1 Taperability

*Taperability* is being used as a metric to compare different ngVLA components and subarrays. Taperability curves show the change in sensitivity versus resolution as parameterized by an inefficiency factor, $\eta_{weigth}$, such that the expected image rms after weighting increases as $\sigma_{rms} = \eta_{weight}\ \sigma_{NA}$. Each taperability curve has a minimum, refered to as the *native* resolution (natural weight and no taper) which gives the highest sensitivity and smallest inefficiency (i.e., by definition an inefficiency $\eta_{weight} = 1$).

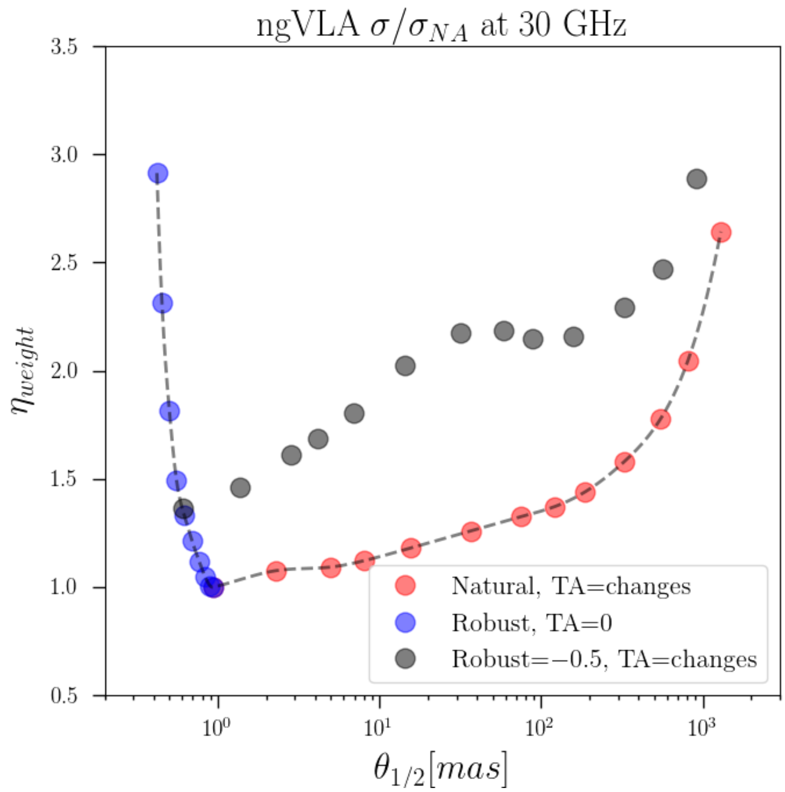


Figure 3: *Taperability* curve for the Main+LBA components of the ngVLA RevD configuration showing the image standard deviation ($\sigma$) at different angular resolutions (FWHM) achieved by varying the imaging weights, simulated at 30 GHz. The noise has been scaled relative to that of the naturally weighted image ($\sigma_{NA}$). The red symbols correspond to use of a uv-taper and natural weights, and the blue symbols to Briggs robust weighting without a taper. The gray symbols are for Briggs robust R= $-0.5$ and a varying uv-taper, which has a large effect on beam quality (see section 2.4.1). The dashed line is the interpolation of the points used to estimate $\eta_{weigth}$.

Figure 3 shows as an example the *taperability* curve of the Main+LBA components of the ngVLA RevD configuration, at 30 GHz. An example description of the simulations and the imaging parameters are presented in ngVLA memo #55 [17] and a *taperability* Python pipeline is available in `https://gitlab.nrao.edu/vrosero/ngvla-taperability-pipeline/`. For the results shown in this document the visibilities were made with the CASA `sm` toolkit using a 4 hr synthesis centered on the transit of a single field at +24 declination. The simulations have a center frequency at 30 GHz and are composed of an integration time of 1 second and a single channel[1]. No source visibilities were predicted, i.e., each simulation is of a blank field. An arbitrary amount of thermal noise was added to the visibilities using the `sm.setnoise` function of the CASA simulation toolkit. The plotted resolutions ($\theta_{1/2}$) correspond to the geometric mean of the minor and major beam FWHM for each simulation. The inefficiency factor ($\eta_{weigth}$) can be estimated at any frequency by scaling $\theta_{1/2}$ with frequency as $\theta_{1/2@30GHz} = \theta_{1/2@\nu} \times (\nu/30\,\mathrm{GHz})$, where $\theta_{1/2}$ is in mas.

*A high degree of taperability (i.e., a shallow curve, thus a low penalty in sensitivity) is desirable because it means the array can accommodate a wide range of science cases.* In this example, when using natural weighting with uv-taper it appears that the variation in sensitivity is small and smooth over a range of angular resolutions: one can move to the right of native by 2 orders of magnitude in resolution while in the left direction only around a factor of 2 before paying a penalty in sensitivity $\gtrsim$2. The reason of the curve's shallowness is related to the array having a large ratio of short baselines to long baselines, thus applying a taper does not down-weight a considerable amount of data. This makes sense since the LBA provides less long baselines when compared with the shortest baselines from the inner subarrays, thus when using small uv-tapers we are not losing much sensitivity. Additionally, when using robust values close to uniform without uv-taper the lost in sensitivity is very high and steep since we are downgrading the shortest baselines which make most of the total amount of baselines. From Figure 4 we can see that the full complement of ngVLA 18 meter antennas (Main+LBA; pink curve) has a very high degree of taperability, i.e., it can be used over a large range of resolutions without a great loss of sensitivity ($\eta_{weight} \leqslant 2$; e.g., ngVLA memo #55 [17]).

## 2.2 Subarrays

Figure 4 shows a compilation of the taperability curves for all the ngVLA components and some selected subarrays (as listed in Table 1). This figure shows that the ngVLA configuration covers an impressive range of resolutions spanning ∼4 orders of magnitude. Also, it demonstrates the advantage of subarrays at extreme resolutions or to obtain greater efficiency at specific intermediate resolutions (i.e., each subarray is efficient over a narrow resolution range).

As previously presented, values at resolutions lower than the native resolution (i.e., to the right of the curve's minimum) are the results from simulations using natural weighting plus a uv-taper; values at resolutions higher than native used robust weighting and no taper. Note that some of these arrays, when used with

[1]MFS simulations for the ngVLA are currently under study.

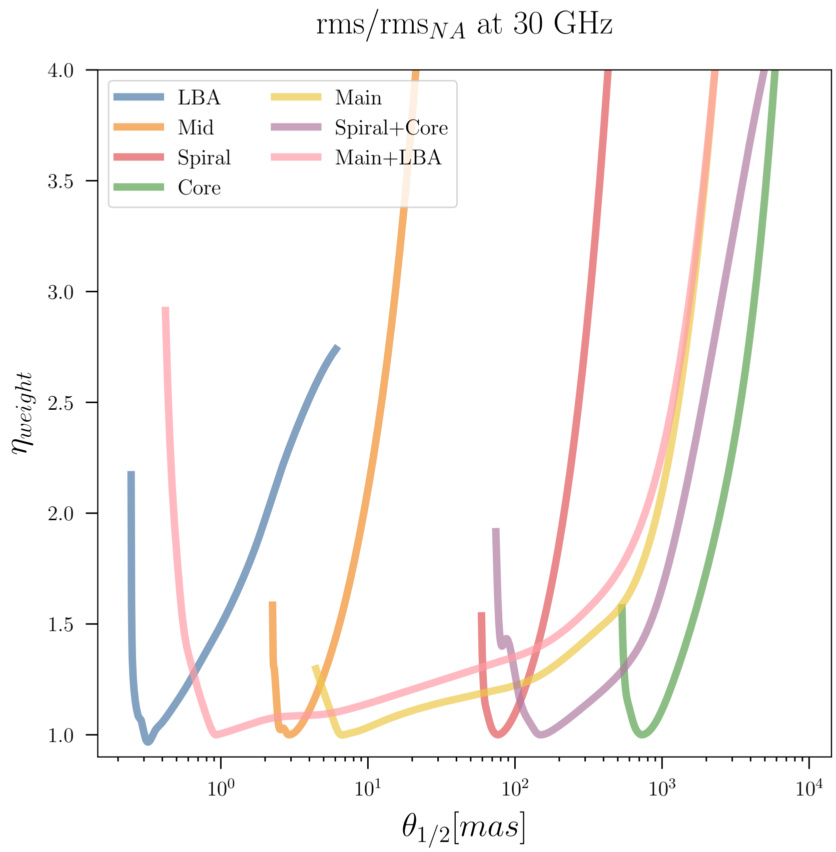


Figure 4: Taperability curves for the ngVLA components and selected subarrays showing the relative sensitivity (image rms compared with the naturally weighted image) vs. 30 GHz resolution. Note that some of these arrays, when used with natural weighting, have non-Gaussian PSF features (e.g., broad PSF skirt) that may be unsuitable for some science cases (see ngVLA memos #55 [17] and #72 [19] about PSF details of these specific arrays).

natural weighting, have non-Gaussian PSF features (e.g., broad PSF skirt) that may be unsuitable for some science cases (see ngVLA memos #55 [17] and #72 [19] about PSF details of these specific arrays). Therefore, beam sculpting will also be necessary and will introduce another source of inefficiency in addition to the taperability that has been discussed this far.

## 2.3 Simulated Resolution and PSF

The physical placement of the antennas is important to achieve a good uv-coverage, which is directly related to the PSF or the "dirty beam". The PSF is a good measure of the performance of an imaging system, providing an insight of the type of errors and artifacts that will appear in the raw images (e.g., [22]). One desirable is the minimization of image-domain sidelobes arising from incomplete sampling. Deconvolution imaging techniques, in principle, enable the removal of the effect of the dirty beam (i.e., sidelobes, skirts, etc), but the current algorithms are limited by the features of poor PSFs.

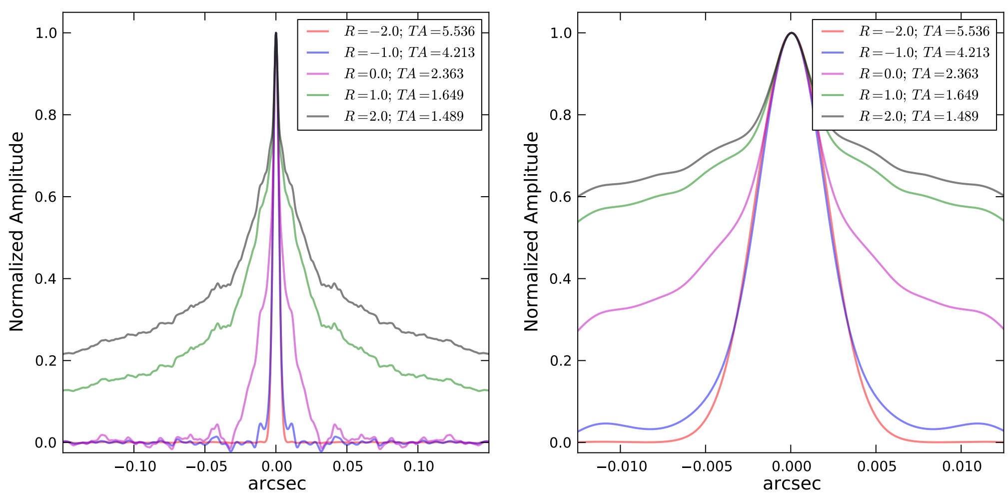


Figure 5: Examples of simulated 100 GHz PSFs, and the effect of different combinations of robust and uv-taper values producing a clean beam size of 5 mas. The PSFs are a selection of the data presented in ngVLA memo #65 [18]. The right panel corresponds to a zoom in of the same PSFs shown in the left panel. Units of taper and resolution are mas.

In the previous section 2.1 it was established that the array configuration of the ngVLA has a high degree of taperability. Unfortunately, arrays with a large ratio of short baselines do not produce desirable PSFs (see Figure 2). Additionally, ngVLA memo #65 [18] shows that different combinations of robust and uv-taper will formally result in PSFs with the same resolution, although the PSF quality may be very different thus affecting the image sensitivity. Figure 5 shows 1D East-West cuts through example PSFs to demonstrate the effect of different imaging weights. All these PSFs have a resolution of ∼5 mas as parameterized by Gaussian fitting in the CASA `tclean` task (see more details about how the algorithm used by `tclean` determines the resolution). However, we can see how combinations of robust and uv-taper values will allow for beams of much higher quality (i.e., more Gaussian), but at the expense of sensitivity as described below.

Figure 6 shows the change in sensitivity with Briggs robust for all the images that have a resolution of ∼5 mas presented in ngVLA memo #65 [18], where $\eta_{weight}$ is an inefficiency factor defined as $\sigma/\sigma_{NA}$. As we can see, from the examples shown in Figure 5 that have more Gaussian-like beams the image noise increases as much as by a factor of ∼3.7 for combinations of robust and uv-taper, but some combinations yield beams with a more reasonable penalty in sensitivity of the order of ∼2 that could have a suitable quality for the scientific requirements.

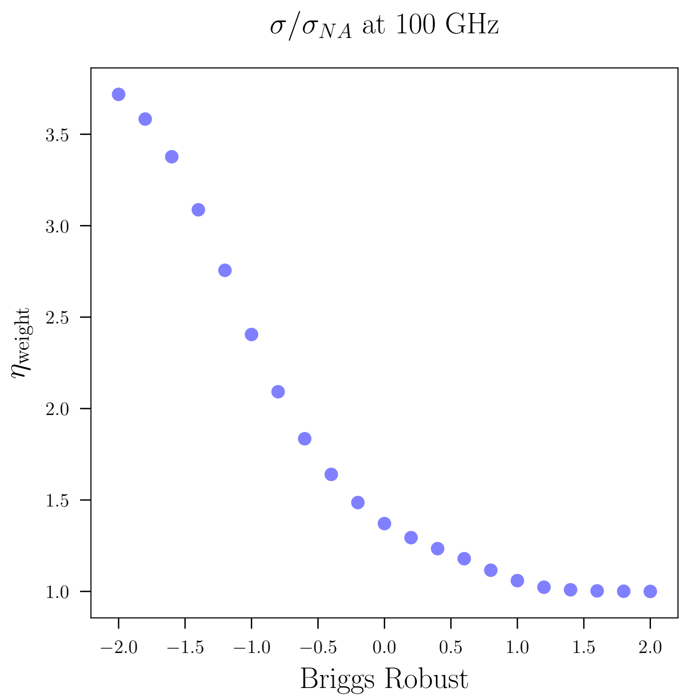


Figure 6: Change of sensitivity with Briggs robust for images with clean beam size of ∼5 mas achieved by varying the imaging weights, simulated at 100 GHz. The data is presented in ngVLA memo #65 [18] .

## 2.4 Beam Sculpting

Here we explore two options for beam sculpting: i) through combinations of imaging parameters (i.e., robust and uv-taper) and ii) by selection of efficient subarrays. It is important to point out that *the need for beam sculpting may vary depending of the scientific requirements and should be studied carefully for each case.*

### 2.4.1 Combination of Imaging Parameters

Specific scientific cases may need to adjust the uv-weighting and other image parameters to sculpt a synthesized beam in order to meet specific science requirements, e.g., image fidelity. As previously presented, the red symbols in the taperability curve shown in Figure 3 are simulations using natural weighting + TA values which enables one to achieve a desired resolution while paying a penalty in sensitivity. Figure 7 shows examples of 1D East-West cuts through selected example PSFs from the simulations performed for that specific curve (i.e., using the ngVLA Main+LBA components). Such figure shows that the resulting PSF for simulations using natural weighting + TA values may not be acceptable[2] (e.g., broad skirt as seen in Figure 7 gray PSFs) for several scientific requirements. With that in mind, a value of Briggs robust R= − 0.5 (represented by the gray symbols in the taperability curve shown in Figure 3) is used as an approximation example of beam sculpting. As we can seen in Figure 3 an additional penalty in sensitivity is added when doing so. However, when using Briggs robust values approaching to uniform the resulting PSFs start to appear more Gaussian-like (see blue PSFs in Figure 7).

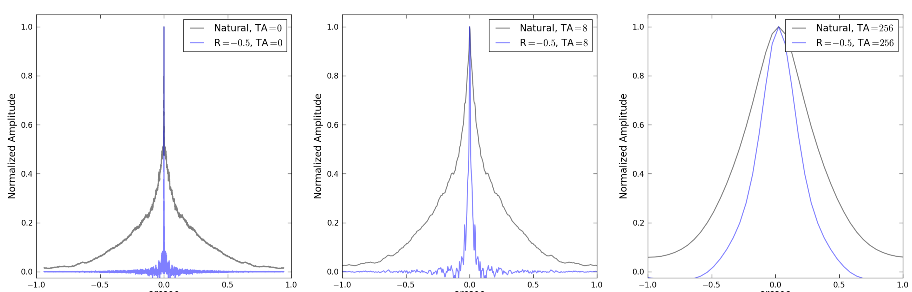


Figure 7: Simulated 30 GHz PSFs for the present ngVLA reference array over a range of resolutions, showing the effect of different imaging weights (TA: uv-taper in mas, R: Briggs robust parameter). These examples illustrate how combinations of robustness and tapering allow for a beam of much higher quality (but at the expense of sensitivity). Units of taper and resolution are mas.

PSF metrics are useful to quantify the quality of the beams and can be used to inform decisions about how to 'sculpt' the synthesized beam to something suitable to a specific science goal. Several PSF quality metrics were studied in ngVLA memo #65 [18]. Specifically, we have been extensively using a metric

[2]Although this may change depending of the selected subarray (see ngVLA memo #55 [17]).

that measures the level of the PSF at a radius of one FWHM (defined in ngVLA memo #65 [18] as 'metric 2b'). Figure 8 shows an example of two radial-averaged PSF profiles for R = −1 and R = 0 with the same reported angular resolution (i.e., 5 mas) and their resulting values for metric 2b (i.e., 12% and 45% for R = −1 and R = 0, respectively). It was suggested in ngVLA memo #47 [7] that a skirt which raises the PSF to a level of 10% at a radius of one FWHM (i.e., metric 2b) may be acceptably low (for comparison, a Gaussian beam is ∼6% at a radius of one FWHM).

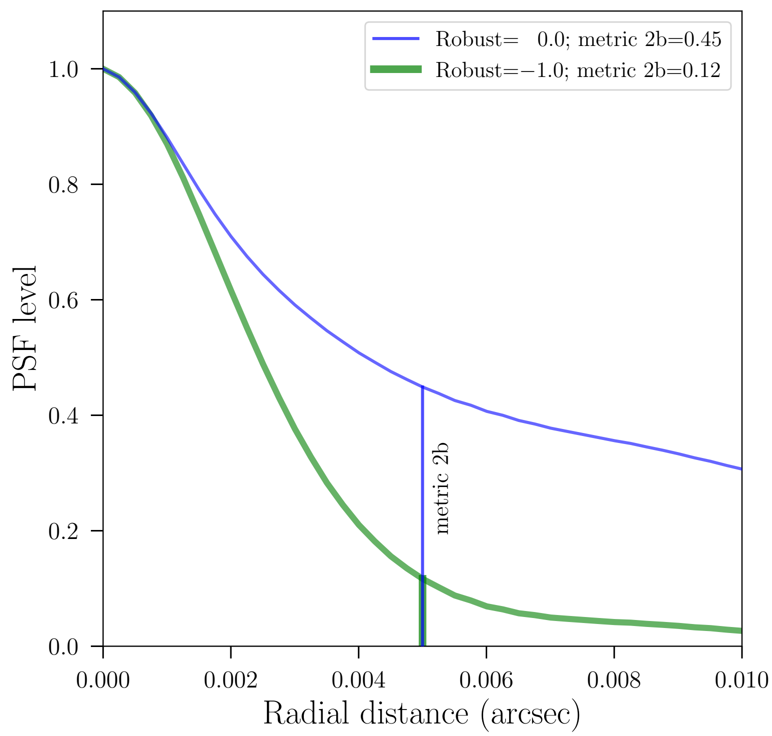


Figure 8: Radial-averaged PSF profile for $R = -1$ and $R = 0$ showing examples for the same angular resolution (i.e., 5 mas). Metric 2b calculates the PSF level at a radial distance of one FWHM.

Figure 9 shows the values of metric 2b as a function of Briggs robust values for PSFs with the same reported angular resolution (i.e., 5 mas; see ngVLA memo #65 [18] for details). Metric 2b is sensitive to a type of PSF non-Gaussianity which is often referred to as a beam 'skirt' or 'plateau'. The gray solid line represents the level value of a Gaussian beam at a radius of one FWHM, i.e., ∼6%. At this radius, for the examples shown in Figure 5 the beams with Briggs robust values $R \gtrsim 0$ are far above 10%, but drop to below or about 10% when a robust value of $R \lesssim -1$ is used (also seen in Figure 8). This 'sculpting' of a more Gaussian beam comes at a cost of sensitivity as shown in Figure 6. The complete data set is presented in ngVLA memo #65 [18].

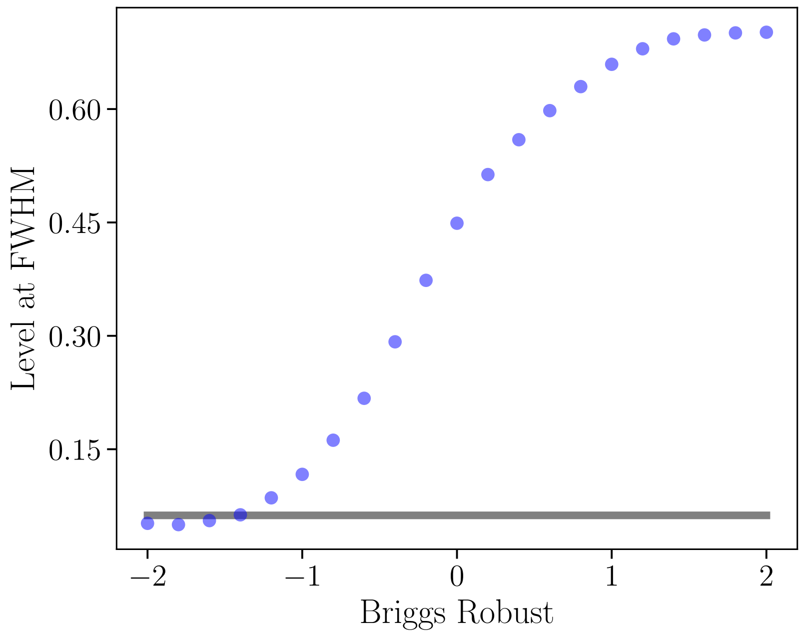


Figure 9: Metric 2b as a function of Briggs robust values of PSFs with angular resolution of 5 mas. The gray solid line represents the level value of a Gaussian beam at a radius of one FWHM, i.e., ∼6%. The complete data set is presented in ngVLA memo #65 [18].

#### 2.4.2 Selection of Subarrays

An alternative method to reduce the level of the PSF skirt is to select a subarray where the number of short baselines is not as large when compared with the amount of longer baselines. A study presented in ngVLA memo #72 [19] shows how different subarrays (specifically, subarrays including different fractions of the Core) can be more efficient at certain resolutions. Figure 10 shows radially-averaged PSF profiles[3]; spline interpolation is used to determine the level of the PSF at a radius of one FWHM (i. e., metric 2b) as marked by the dashed lines. This figure demonstrates the reduction of the skirt depending on the selected subarray.

[3]Radially-averaged profiles are produced using the 3rd party CASA task `iring`, obtained from the ALMA Nordic Node.

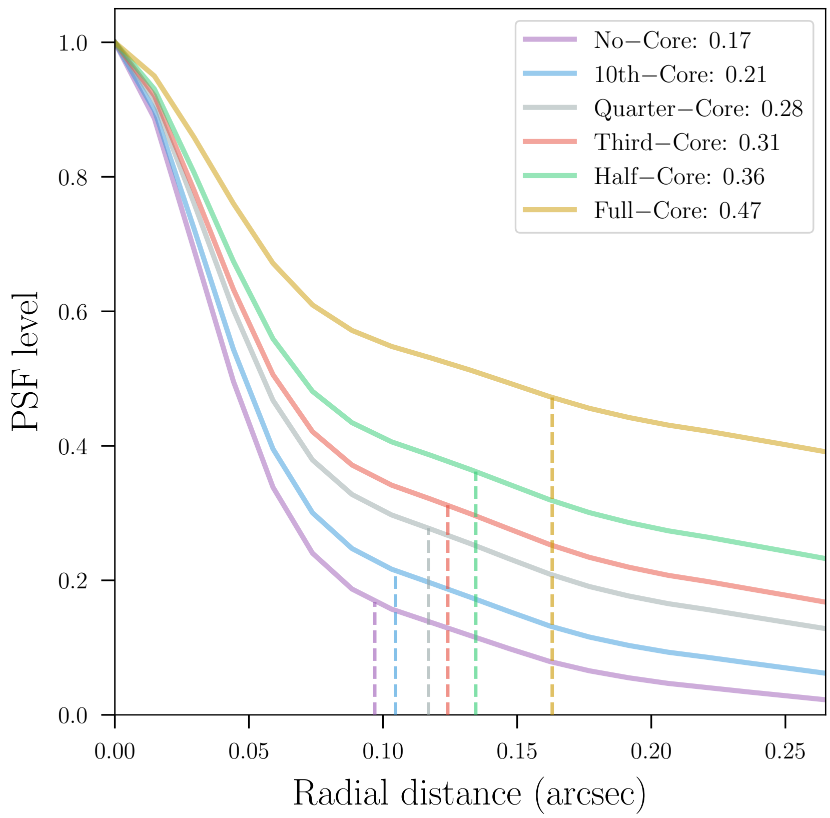


Figure 10: Radially-averaged PSF profiles of the naturally weighted synthesized beam (solid lines) for six subarrays that includes the Spiral subcomponent plus different fractions of the Core. Spline interpolation is used to determine the level of the PSF at a radius of one FWHM as marked by the dashed lines.

Figures 11 shows the values of each taperability curve (when using fractions of the Core; see ngVLA memo #72 [19]) at selected constant resolution values between 75 mas and 1 arcsec. This abscissa is labeled according to the number of core antennas in the subarray (bottom axis) and the corresponding name given to the subarray (top axis); linear interpolation is used between each simulated subarray. Figure 11 makes it clear that different subarrays are more efficient at different resolutions. Subarrays with fewer antennas in the core have higher native resolutions and therefore suffer less of a sensitivity penalty when using image weights to achieve a higher resolution PSF. On the other hand, subarrays with more core antennas can be tapered to lower resolutions with less of a sensitivity penalty.

In ngVLA memo #76 [20] we explored the option of selecting subarrays for each driving case of the ngVLA based on the target resolution, LAS requirements and

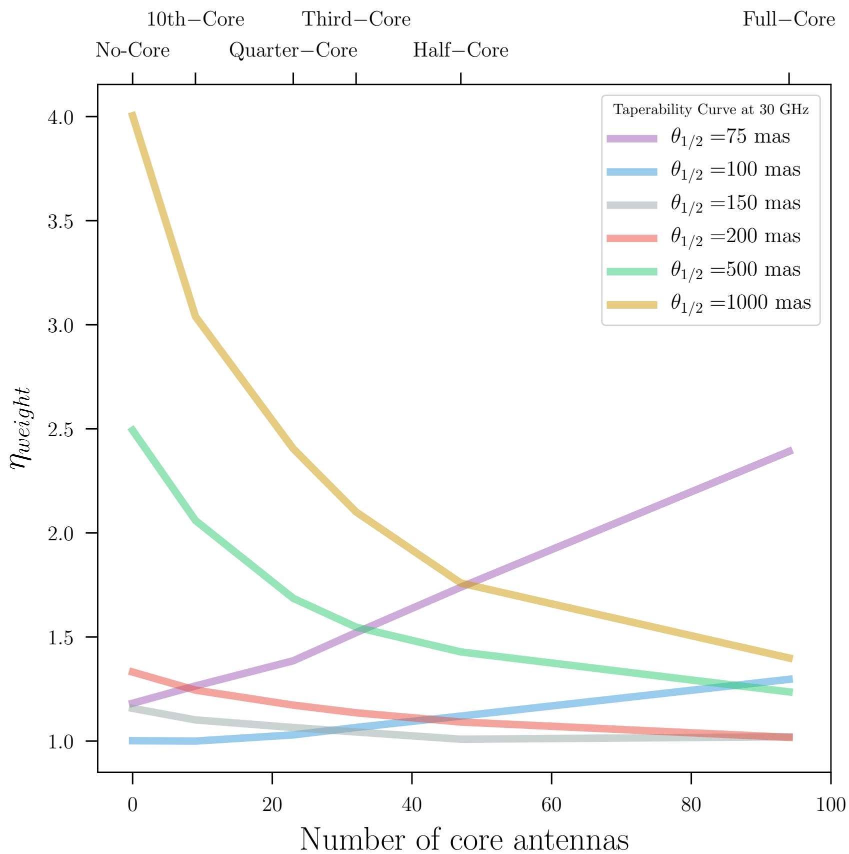


Figure 11: Efficiency curves for different selected resolutions and subarrays for uv-taper and natural weights and Briggs robust weighting without a taper (red and blue data series in the taperability figures).

with the ability to be used within a factor of 2 of its naturally-weighted sensitivity. This is achieved by removing the antennas that would otherwise be heavily down-weighted by either robust or uv-taper (i.e., antennas located within the Core or the mid-baseline subarrays, respectively) with *the additional advantage of freeing up antennas to use by other projects observing simultaneously.*

***In conclusion, subarrays that 'naturally' produce a more Gaussian PSF will require less extreme imaging weights and therefore will incur a less severe sensitivity penalty.***

## 2.5 Sensitivity of the ngVLA

The ngVLA is designed to operate in a frequency coverage of ∼1.2 – 116 GHz in 6 receiver bands. All the values presented in this section account for predictions for the receiver temperature, aperture efficiency, atmospheric conditions and spillover as a function of frequency (see https://ngvla.nrao.edu/page/performance for the specific values at each band). Therefore, these values do not account for atmospheric variation (see more in ngVLA memo #21 [2]) and confusion noise, which would need to be independently considered for some of the combinations of frequency, resolution and sensitivity and will be presented in a coming version of the ngVLA sensitivity calculator. Figures of merit are presented per 1 hour of observation time and intended to be scaled to other observing times.

A key performance table for the Main+LBA ngVLA configuration is presented and remains up to date in the ngVLA website, for all the 6 receiver bands and representative resolutions. A web interface next generation Exposure Calculator Tool (ngECT) is currently being developed based on such investigations and will eventually supersede the values included in the performance metric tables. In the meantime, a sensitivity calculator Python script located at https://gitlab.nrao.edu/vrosero/ngvla-sensitivity-calculator can be used to estimate the performance sensitivity including point source and surface brightness sensitivities for lines and continuum. This calculator makes use of the taperability curves for many representative subarrays of the ngVLA and allows the calculation of the sensitivity at different resolutions.

### 2.5.1 Continuum Point Source Sensitivity

Figure 12 shows the continuum point source sensitivity for 1 hour of observation time, using the maximum continuum bandwidth at the natural resolution (i.e., for untapered, naturally weighted images) for the Main+LBA components. The gray dots show the 1-hour continuum sensitivity using the maximum available bandwidth and the colored lines show the relative change in sensitivity across each band. The maximum instantaneous correlator bandwidth of 20 GHz exceeds the receiver bandwidth at all bands except at band 6. Thus for band 6 we present the continuum sensitivity for three possible settings with central frequencies centered at 80, 93 and 106 GHz. *From Figure 12 we can see that at every ngVLA band it will be possible to make a continuum image with a sensitivity below 1 $\mu$Jy/beam in under 1 hour of observation.*

In Figure 13 we present the continuum sensitivity over a range of resolutions, where we have incorporated the taperability and the point source sensitivity curves (Figures 3 and 12, respectively) together to *show how the sensitivity varies as a function of both frequency and resolution.* This is shown here for the Main+LBA subarray, for which the taperability curve is fairly flat over a few

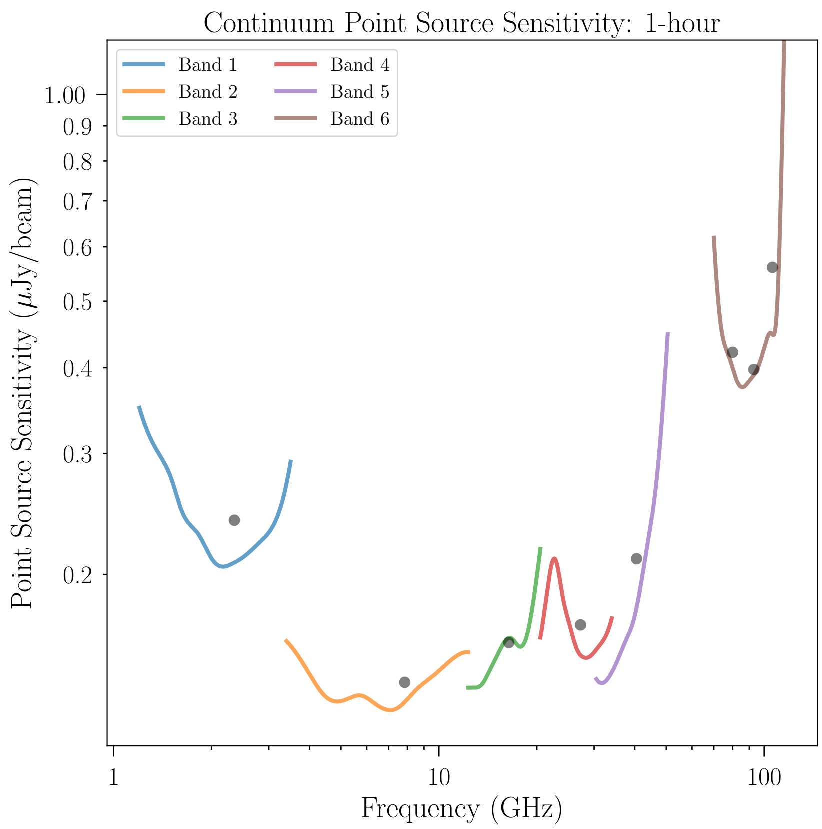


Figure 12: Continuum point source sensitivity of the ngVLA Main+LBA components at the natural resolution. The gray dots show the 1-hour continuum sensitivity using the maximum available bandwidth and the colored lines show the relative change in sensitivity across each band. The maximum instantaneous correlator bandwidth of 20 GHz exceeds the receiver bandwidth at all bands except at band 6.

orders of magnitude in resolution. The white contours are all about or below 1 $\mu$Jy/beam in the 1-hour point source sensitivity, and we can see that they not only extend across the frequency range of each receiver but also over a large range of resolutions. Overall, we can see that the ngVLA will be able to produce sensitive images at angular resolutions almost as small as 0.1 mas at the highest frequency and as large as about 100 arcseconds at the lowest frequency.

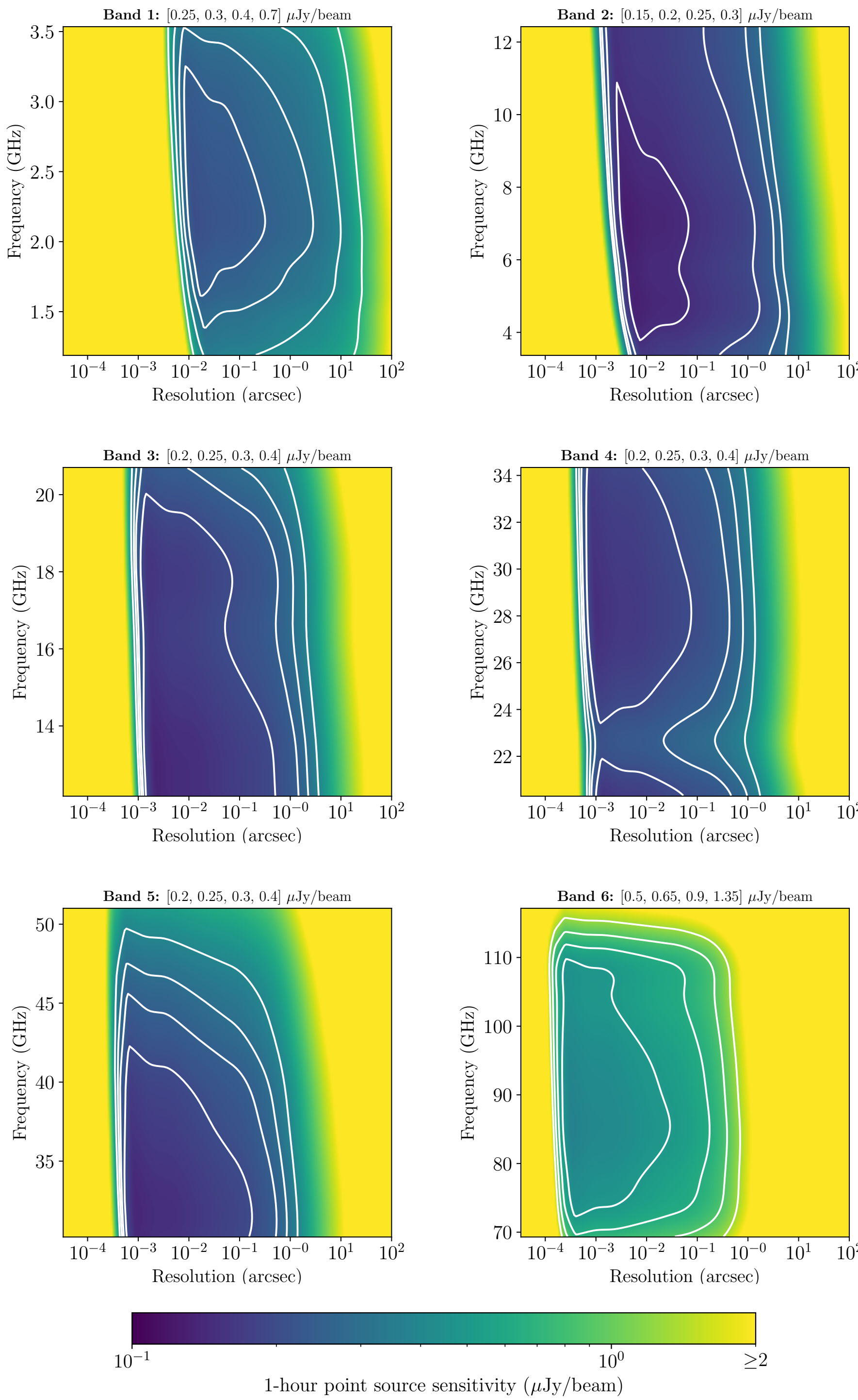


Figure 13: Continuum sensitivity over a range of resolutions incorporating both the taperability and continuum point source sensitivity curves for the Main+LBA components.

### 2.5.2 Line Sensitivity

Similarly, Figure 14 shows the line sensitivity for 1 hour of observation time using a bandwidth of 10 km/s at the natural resolution (i.e., for untapered, naturally weighted images) for the main+LBA subarray. Figure 15 shows the line sensitivity over a range of resolutions, where we have incorporated the taperability and the line sensitivity curves (Figures 3 and 14, respectively) together to show how the sensitivity varies as a function of both frequency and resolution.

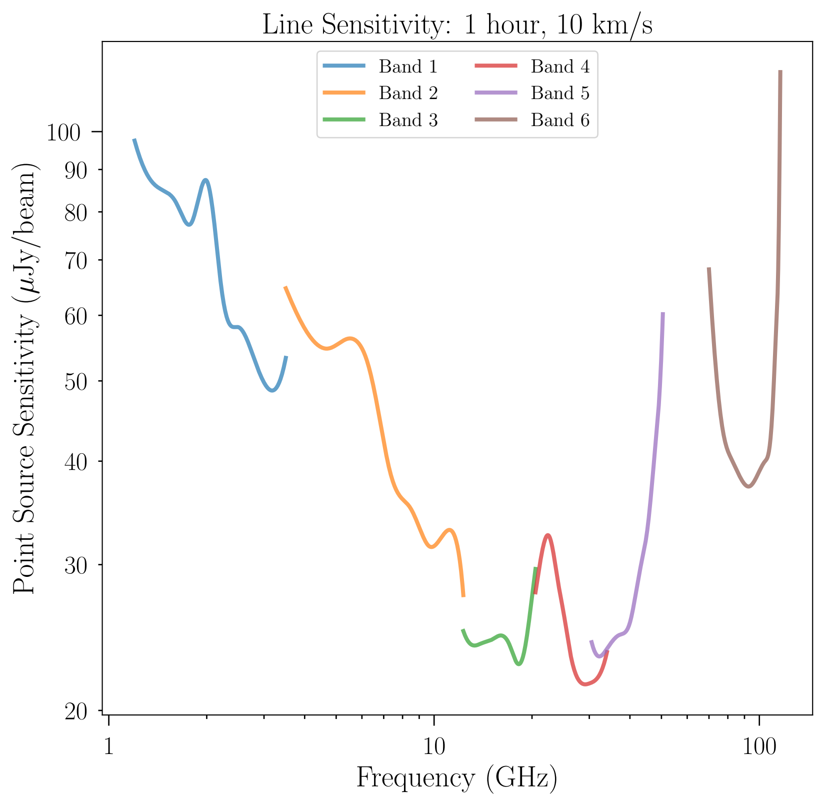


Figure 14: Line sensitivity at the natural resolution for 1 hour of observation and 10 km/s of bandwidth.

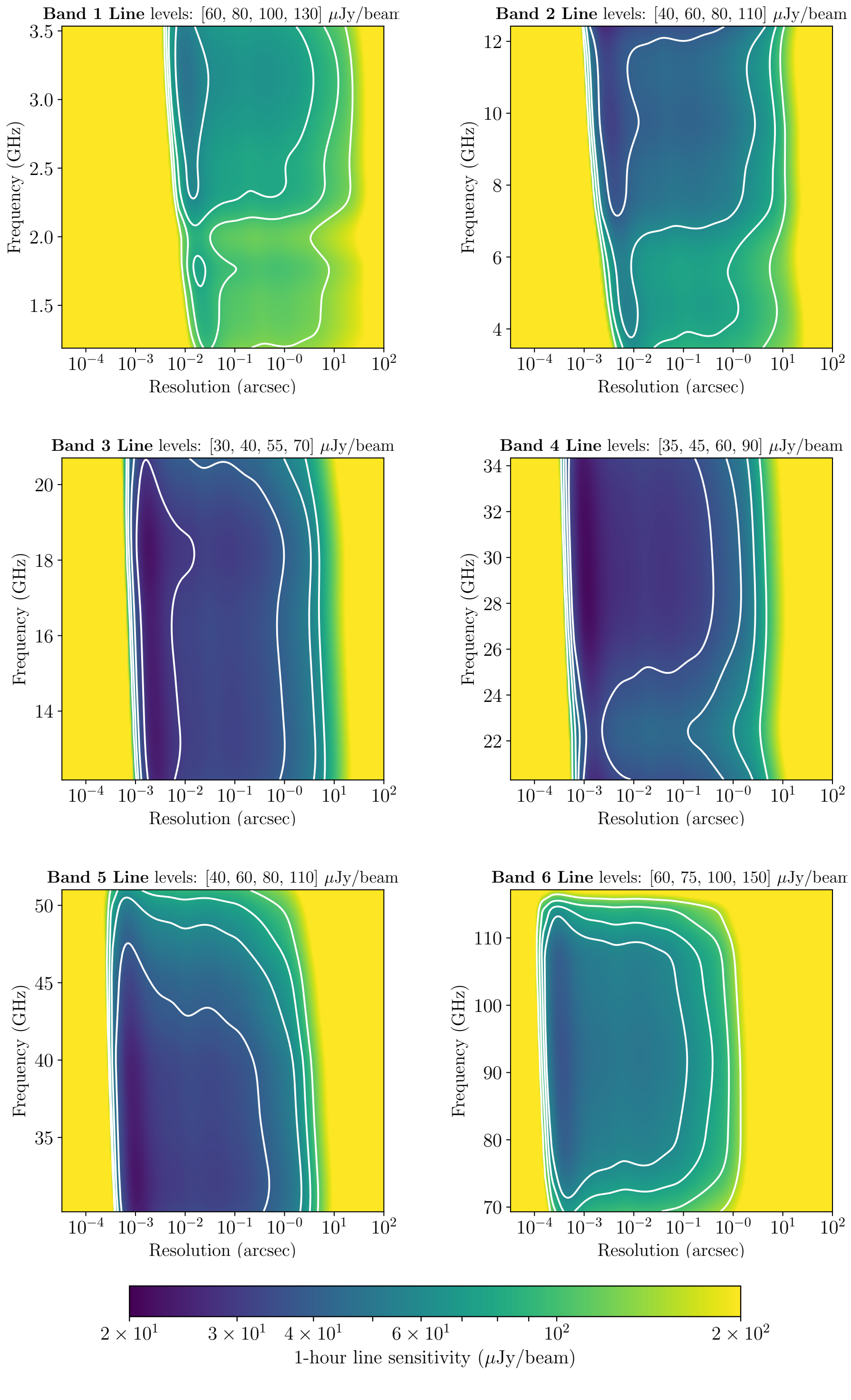


Figure 15: Line sensitivity over a range of resolutions incorporating both the taperability and line sensitivity curves for the main+LBA subarray.

### 2.5.3 Continuum Brightness Sensitivity

Additionally, Figure 16 shows the continuum brightness sensitivity for 1 hour of observation time, using the maximum continuum bandwidth at a resolution of 1 arcsec for the main+LBA subarray. We can see how the sensitivity changes with frequency as a factor of $\sim \nu^{-2}$, with band 6 achieving a brightness sensitivity of $\sim$0.3 mK in 1 hour observation. Figure 17 shows the continuum brightness sensitivity over a range of resolutions, where we have incorporated the taperability and the continuum brightness sensitivity curves (Figures 3 and 16, respectively) together to show how the sensitivity varies as a function of both frequency and resolution.

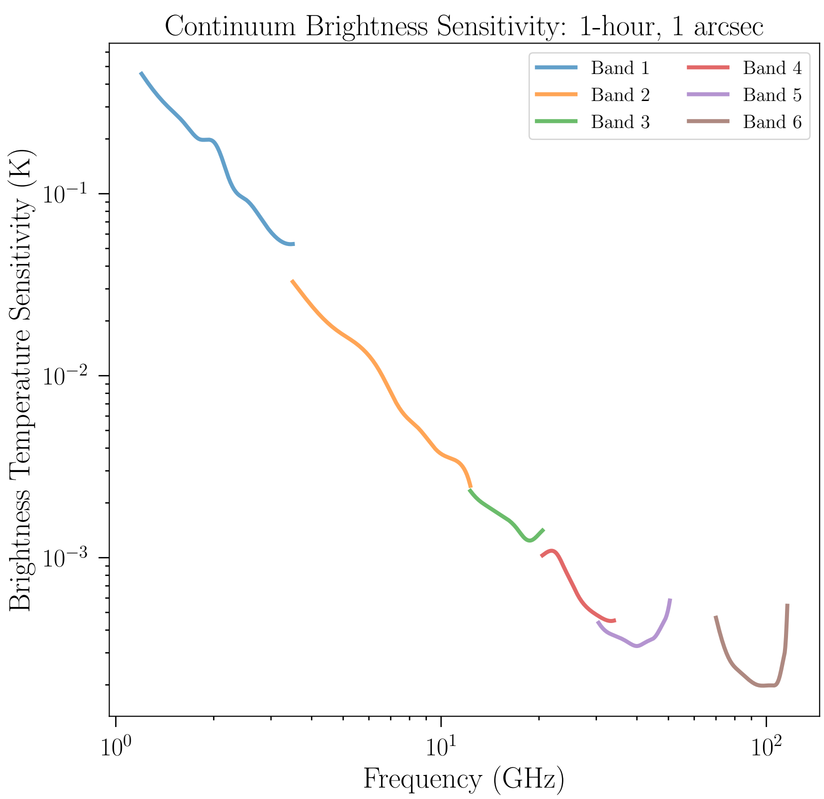


Figure 16: Continuum brightness sensitivity for 1 hour of observation and 1 arcsec resolution.

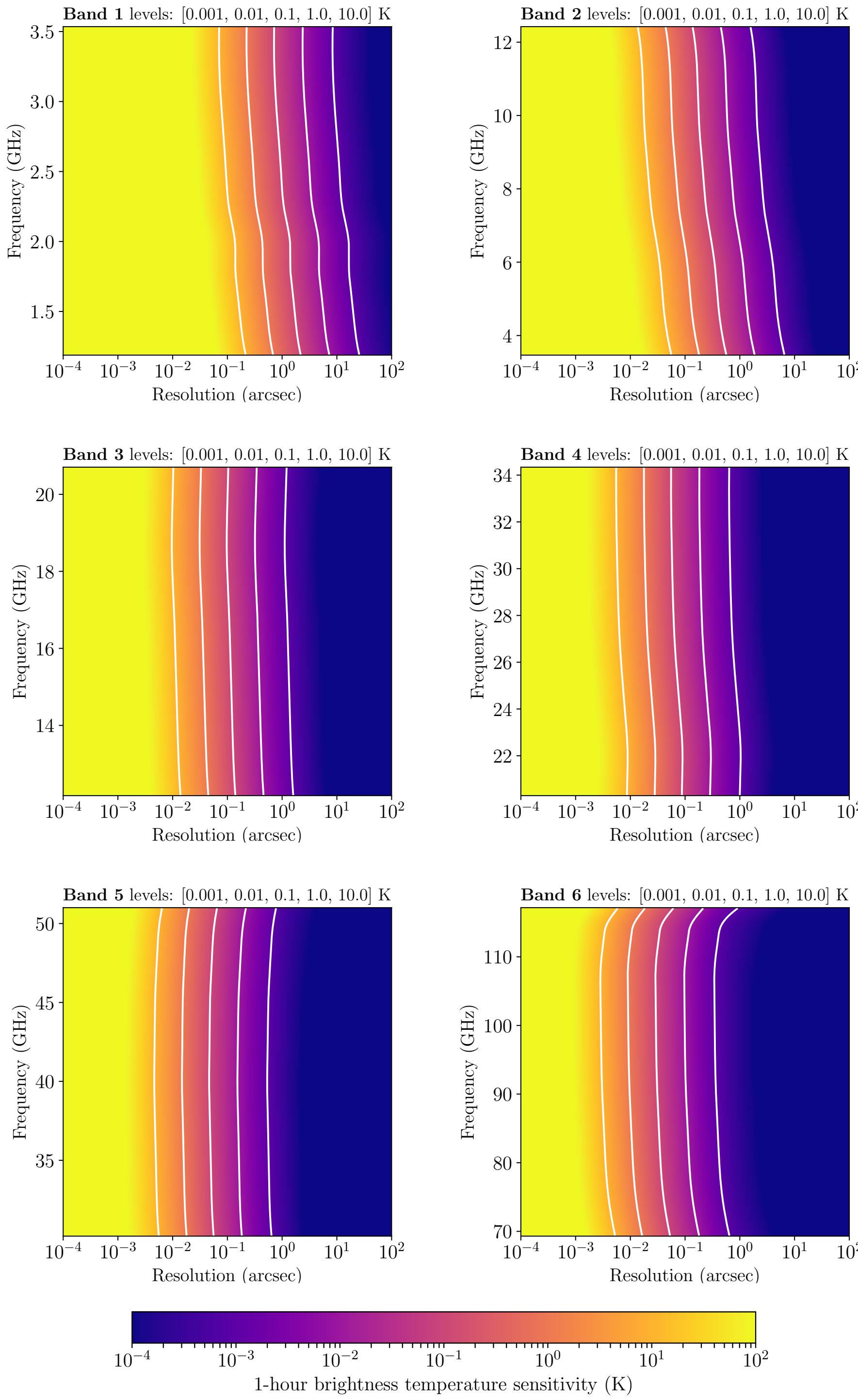


Figure 17: Continuum brightness sensitivity over a range of resolutions incorporating both the taperability and continuum brightness sensitivity curves for the main+LBA subarray.

### 2.5.4 Line Brightness Sensitivity

Figure 18 shows the line brightness sensitivity for 1 hour of observation time and using a bandwidth of 10 km/s at a resolution of 1 arcsec for the main+LBA subarray. Figure 19 shows the line brightness sensitivity over a range of resolutions, where we have incorporated the taperability and the line brightness sensitivity curves (Figures 3 and 18, respectively) together to show how the sensitivity varies as a function of both frequency and resolution.

For all the figures that show the contours of the change of sensitivity with frequency and resolution we can see the resolution range shift with frequency, from the higher resolutions (band 6) to the lower resolutions (band 1). This is due to the natural resolution (i.e., the untapered, naturally-weighted resolution) scaling with wavelength.

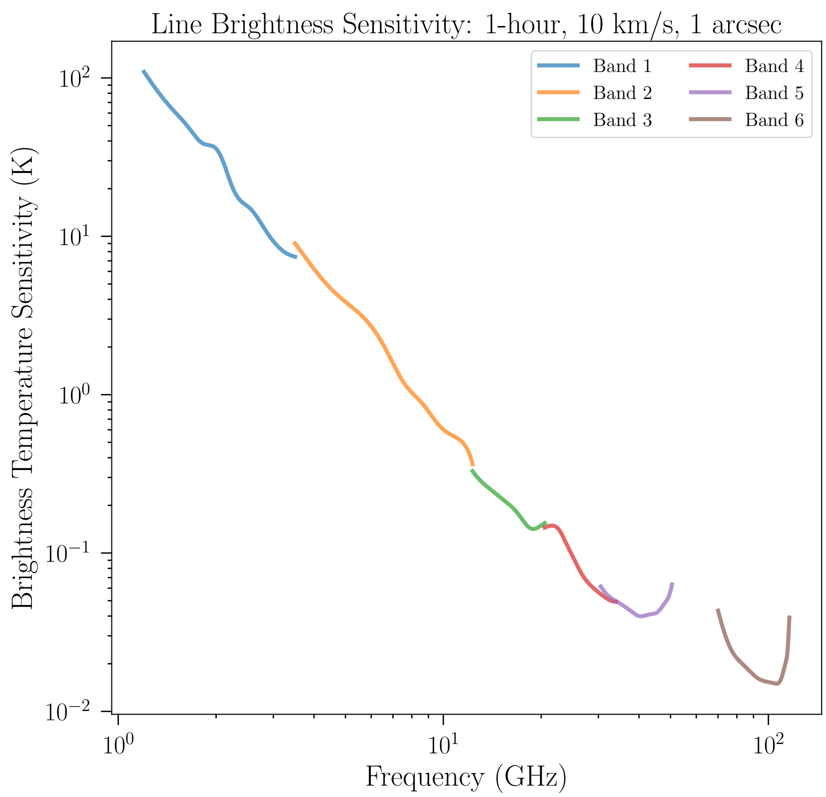


Figure 18: Line brightness sensitivity for 1 hour of observation and 10 km/s and 1 arcsec resolution.

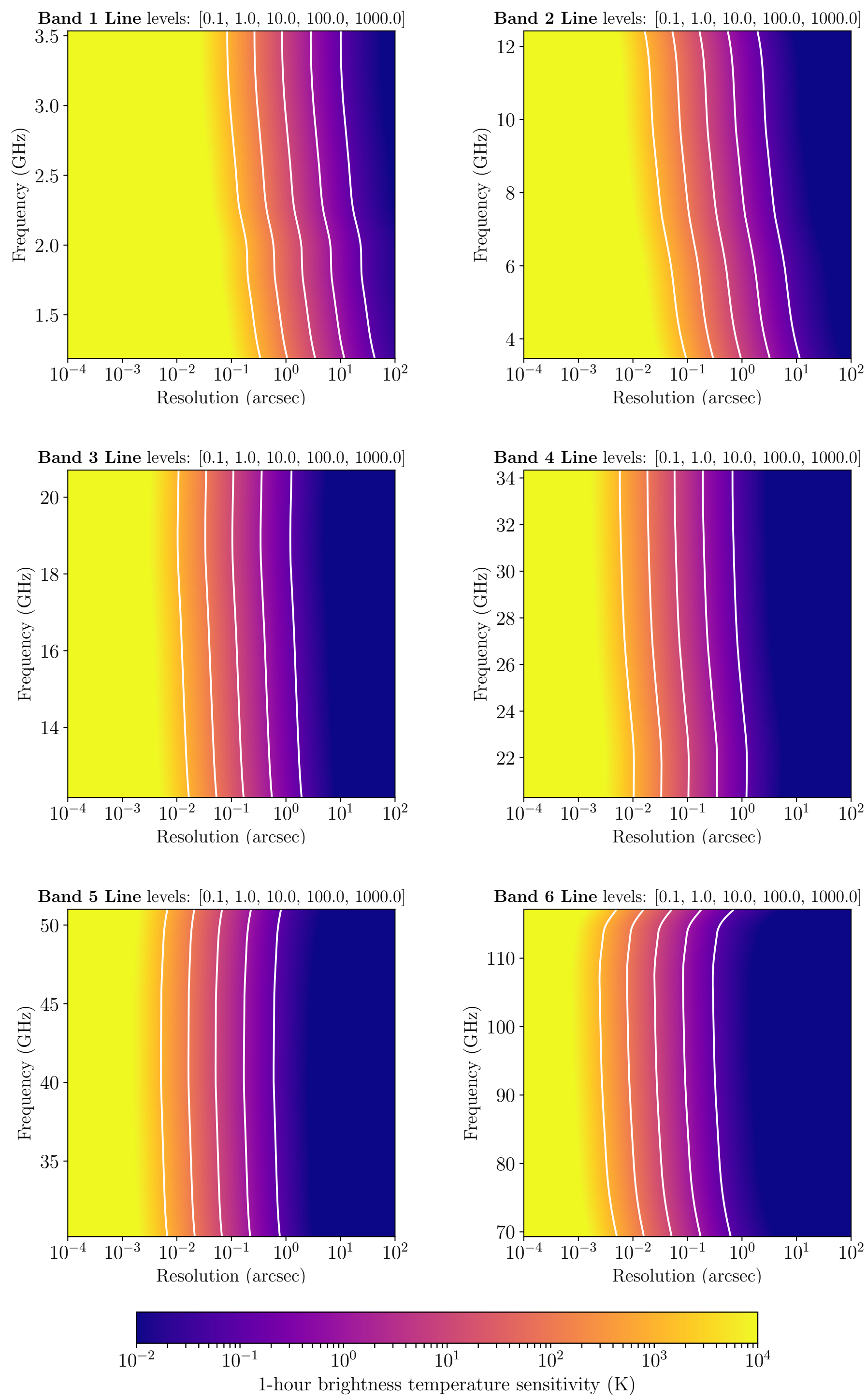


Figure 19: Line brightness sensitivity over a range of resolutions incorporating both the taperability and line brightness sensitivity curves for the main+LBA subarray.

# 3 Image Fidelity

Image fidelity is used as a measure of image correctness and is defined here as the comparison of the model (or the 'correct image') with the resulting image (or the 'produced image'), such that a high fidelity image has smaller residuals after subtracting the model from the image.

In this work we use the definition of fidelity given in equation 1, as defined in ngVLA memo #67 [12] and also presented in the ngVLA Science Requirements document [13]:

$$F = 1 - \frac{\Sigma_i[\beta_i W_i * (|I_i - M_i|)]}{\Sigma_i \beta_i^2 W_i} \tag{1}$$

where $I$ is the resulting image and $M$ is the model. Additionally, $\beta_i$ is defined to be $\max(|I_i|, |M_i|)$ and $W_i$ is a 'window function' which defines the region where the fidelity is evaluated ($W_i = 0$ outside and $W_i = 1$ inside). For more details about this image fidelity definition see ngVLA memo #67 [12].

One of the main challenges to measure image fidelity is related with the scarcity of a representative model of the correct image for the majority of real scientific observations. Following, we present simulated images and examples of image fidelity calculations for two of the ngVLA KSGs, i.e., KSG 1 Protoplanetary Disks and KSG 3 Imaging Molecular Gas in Nearby Galaxies, as presented in ngVLA memos #65 [18] and #89 [21], respectively.

## 3.1 KSG 1: Protoplanetary Disks

ngVLA memo #65 [18] presents a systematic study on image fidelity analysis for imaging of protoplanetary disks to determine the combination of imaging parameters that provides the optimal balance between PSF quality and sensitivity. Following, we summarize the procedure and results.

### 3.1.1 Model and Simulations

For the simulations of the ngVLA observations, we employ the ngVLA Main interferometric subarray (ngvla-main-revC.cfg)[4], which is composed of 214 18 m antennas. We adopt the same model used in ngVLA Memo #33 [14], namely, 'Imaging Planetary Systems in the Act of Forming with the ngVLA' by Ricci et al. 2018a [15] and Ricci et al. 2018b [16]. The model image, shown in Figure 20, is at 3 mm and the disk is at +24° Declination, which corresponds to the declination of the nearby Taurus star forming region. Ricci et al. 2018b [16] presents in detail information about the creation of the synthetic image of the model for the continuum emission and all the physical parameters that they

[4]Note that ngVLA memo #65 [18] uses RevC array configuration.

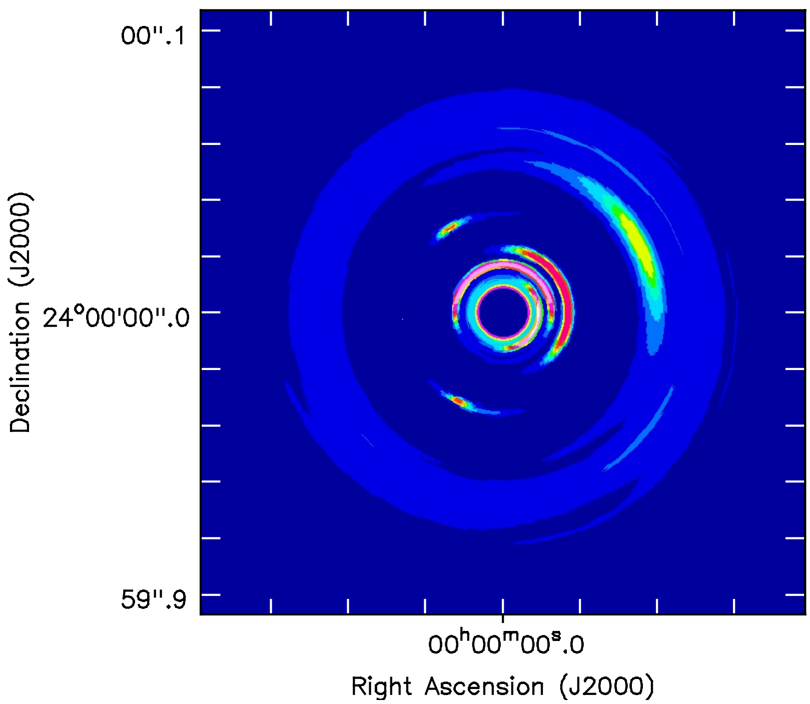


Figure 20: Synthetic model image for a planetary disk at 3 mm from KSG 1. Model credit: Ricci et al. 2018a [15] and Ricci et al. 2018b [16].

adopted.

For the simulations, we generated the visibilities with CASA task `simobserve` and using 8 hr synthesis centered on transit. The simulations have a center frequency of 100 GHz and are composed of 1 channel with a bandwidth of 10 GHz and an integration time of 60 s[5]. Thermal noise was added using the `sm.setnoise` function of the `sm` toolkit with a '*simplenoise*' parameter[6] of 0.9 mJy which corresponds to an rms level of $\sim 0.2\,\mu$Jy/beam in the final natural and untapered continuum image. From ngVLA memo #55 [17], we find that the untapered, naturally weighted point source sensitivity of the Main interferometric array at 93 GHz is $0.83\,\mu$Jy/beam for a 1 hour observation[7]. Therefore,

[5]We choose this integration time in order to keep the measurement set files small. Time smearing is not an issue for simulated observations, but this value would need to be reconsidered before scheduling actual observations.

[6]For more on estimating the expected rms noise in an untapered, naturally-weighted Stokes I image and adding thermal noise to a MS see https://casaguides.nrao.edu/index.php/Simulating_ngVLA_Data-CASA5.4.1

[7]Since the system temperature have been averaged at each band, we assume that the continuum rms of the images at 93 GHz and 100 GHz are the same.

an rms value of $\sim 0.2\,\mu$Jy/beam corresponds to on-time integrations of about $\sim 17$ hr with the ngVLA.

### 3.1.2 Determination of Imaging Parameters

A fundamental requirement of KSG 1 is to achieve a spatial resolution of 5 mas at 100 GHz. Therefore, in order to investigate what combination of imaging parameters will produce such resolution, we made a grid of PSFs using a range of Briggs weighting and UV-tapers. We vary the robust value from uniform ($R = -2$) to natural ($R = 2$) in steps of 0.4 (for a total of 11 values of robust) and use values of uv-taper from 0 to 6 mas in steps of 0.5 mas (for a total of 13 values of uv-taper) resulting in a grid of 143 images. The imaging was done using CASA task `tclean` and all the simulated images have an image size of

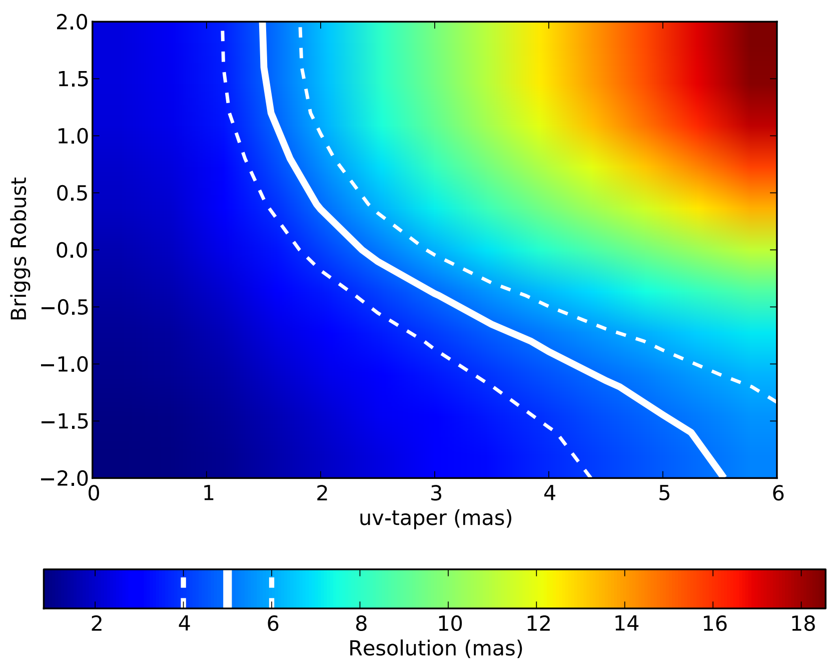


Figure 21: Resolution as a function of the robust and uv-taper values. The color scale shows the size of the clean beam as fit with the CASA `tclean` task. The solid white line are the combination of robust and uv-taper values that will result on a resolution of 5 mas, and the dashed lines delimit the resolutions from 4 to 6 mas.

5120 px. Figure 21 is a color contour representing the achieved resolutions[8] of the resulting PSFs from our grid using different Briggs robust values and uv-tapers. The combinations of Briggs robust and uv-taper values that result in a resolution of 5 mas is represented by the white solid line.

#### 3.1.3 Images with the Desired Resolution

The results from Section 3.1.2 show that there are many combinations of robust and UV-taper that will produce a 5 mas clean beam. Although different combinations will formally result in the same resolution, other properties of the resulting PSFs may be very different. Different combinations of robust and UV-taper will also affect the image sensitivity (for more details see section 2.3). For this study, we create new simulated images using only combinations of Briggs weighting and UV-taper which will give 5 mas resolution. We vary the robust value from uniform ($R = -2$) to natural ($R = 2$) in steps of 0.2 in order to have a suite of 21 equally spaced values. We pair each robust value with a uv-taper based on interpolation of the white solid line shown in Figure 21.

#### 3.1.4 Results

We calculate the fidelity for all the images that have a clean beam size of $\sim$5 mas. Furthermore, we made simulations and images for noisy and noise-free cases. Figure 22, shows the image fidelity as a function of robust value, demostrating how the image fidelity starts decreasing for robust values R$>0$ and R$>0.8$, respectively. At that point, clean is failing to converge due to the broad skirt of the PSF. Note that we used typical, conservative clean parameters that were held constant across the set of images we analyzed. Additional tuning of clean parameters may improve this issue with convergence (e.g., loop gain, cycle niter, multiscale).

For the noise-free and noisy cases we obtain image fidelities of $\sim 95\%$ and $\sim 60\%$, respectively. We find that the fidelity is maximized when using robust R$= -1.4$ for the noisy case and R$\simeq -1.9$ for the noise-free case. Therefore, we conclude that R$= -1.4$ provides the natural balance between PSF quality and sensitivity for this use case. Specifically, for more positive robust values the fidelity decreases due to poor PSF quality (leading to increased deconvolution errors) and for more negative robust values the fidelity decreases because the noise increases.

Figure 23 shows an example of one of the images with high image fidelity corresponding to a R$= -1.6$. The upper panel shows the model image smoothed to a resolution of 5 mas and the lower panel shows the resulting image with R$= -1.6$. Figures 24 and 25 show the magnitude of the residual image, |Image–Model|, for the noise-free and noisy cases, respectively. The contours on the

[8] The plotted resolutions correspond to the geometric mean of the minor and major beam FWHM of the synthesized beam, as parameterized by Gaussian fitting inside the CASA `tclean` task.

residual images trace the main features of the smoothed model image. We can see how the residuals are an order of magnitude smaller for the noise-free case compared to the noisy one and that the residuals in the noisy case are noise-like and do not appear related with the model flux. This indicates that the fidelity in the noisy case is noise limited and not strongly affected by deconvolution errors, and therefore not strongly dependent on the exact choice of cleaning parameters. Such an image appears to satisfy each of the requirements of KSG 1.

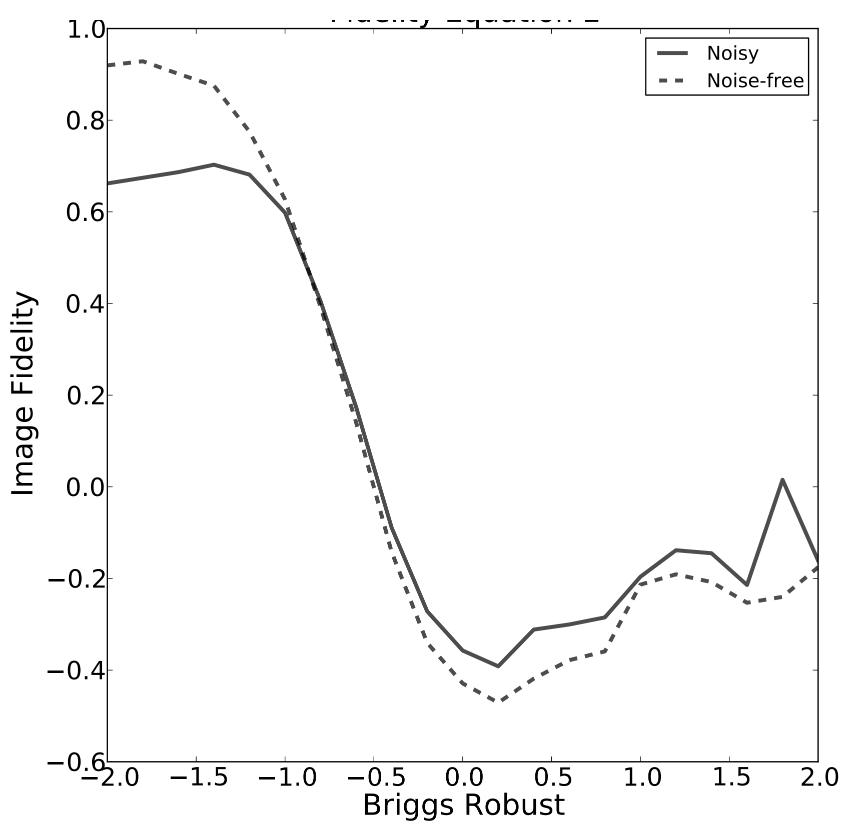


Figure 22: Fidelity vs robust.

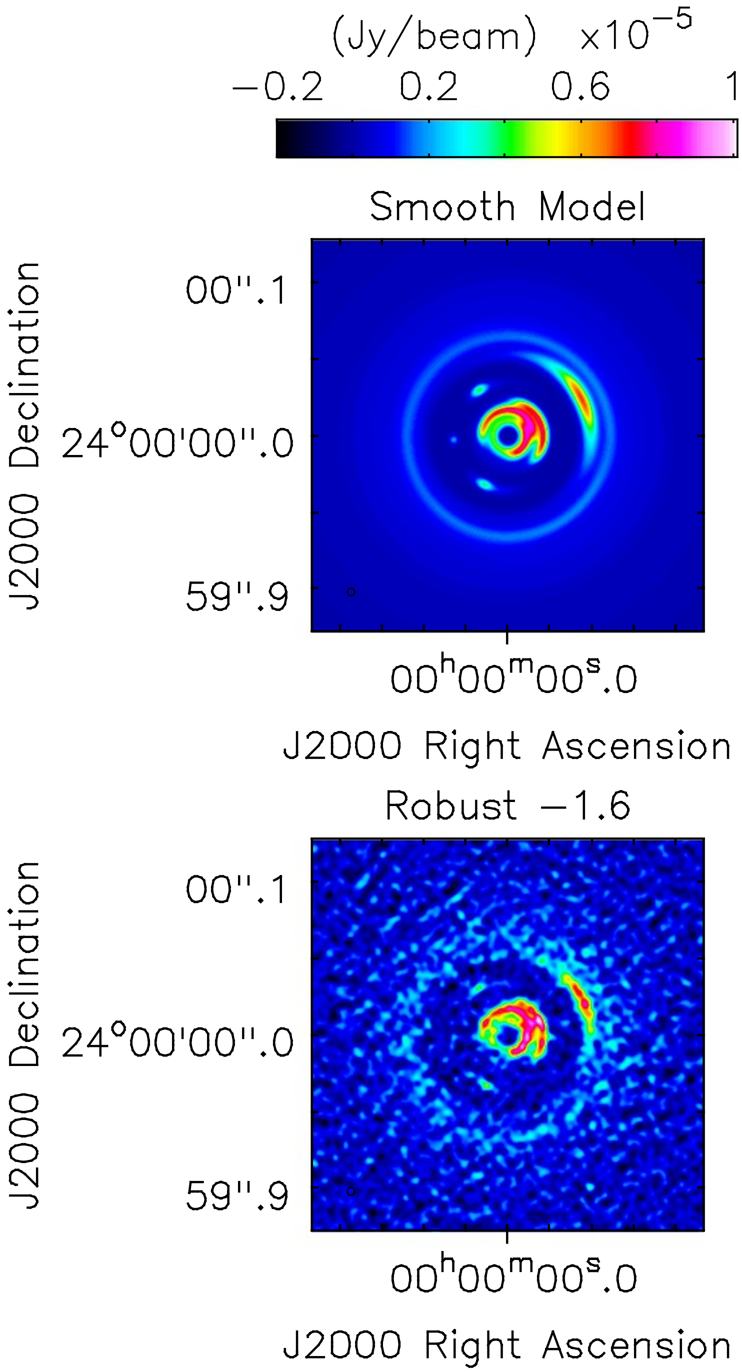


Figure 23: (Upper panel) Smooth model to a 5 mas resolution. (Lower panel) Clean image for R= −1.6.

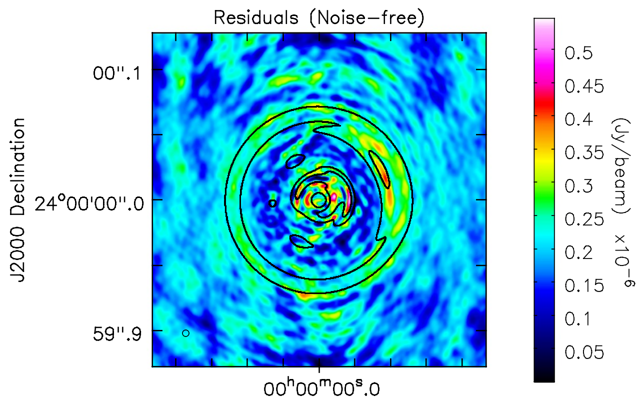


Figure 24: Residuals noise-free image for R= −1.6.

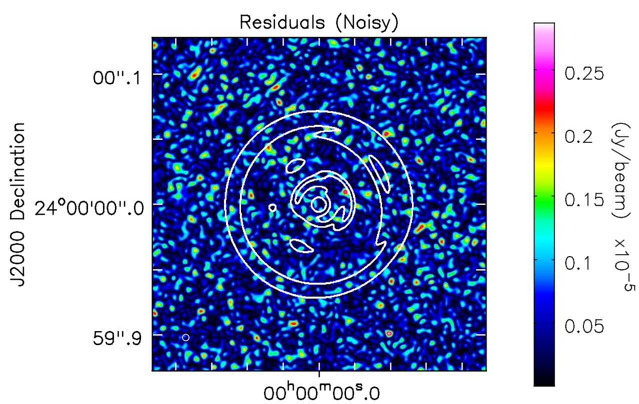


Figure 25: Residuals noisy image for R= −1.6.

## 3.2 KSG 3 (NGA8): Imaging Molecular Gas in Nearby Galaxies

ngVLA memo #89 [21] (and its addendum) presents a study on image fidelity analysis for imaging molecular gas in nearby galaxies. We created a representative simulation that combines observations with several components of the ngVLA, i.e., the Spiral+Core subarray of the Main configuration, the Short Baseline Array, and the Total Power antennas. The simulations use mosaicking to cover a detailed model of a spiral galaxy that is nearly 2 arcminutes in diameter and an appropriate amount of thermal noise was added to the model visibilities. The results demonstrates the capabilities of the ngVLA to achieve high-fidelity imaging for extended and complex sources.
Additionally, an image fidelity pipeline has been developed and can be found in `https://gitlab.nrao.edu/vrosero/ngvla-fidelity-pipeline` (for more details about the pipeline see the addendum of ngVLA memo #89 [21]). Additionally, comparisons of the ngVLA RevC and RevD array configurations are presented in the addendum of ngVLA memo #89 [21]. Following, we summarize the procedure and results of this memo.

### 3.2.1 Model and Simulations

For the model we adopt an observation from the PHANGS-ALMA[9] survey of the spiral galaxy NGC 4321 using ALMA at 230.538 GHz. The image used is a moment map with an image size of 474 X 422 pixels, cell size of 0.5 arcsec, and restoring beam of ∼1.7arcsec. The diameter of the NGC 4321 galaxy is ∼230 arcsec, thus nearly filling up the entire image (field of view ∼3.95 arcmin). In order to use this observation as our model we made several changes to the image file as reported in ngVLA memo #89 [21].

For the simulated observations and given the requirements of the NGA8 use case (i.e., 100mas resolution, LAS=120arcsec), three components of the ngVLA have been adopted: the Spiral+Core subarray of the Main configuration, the Short Baseline Array, and the Total Power antennas (all configurations from the ngVLA RevC array configuration). A mosaic pattern is implemented for the Spiral+Core and SBA configurations to cover the large angular size of nearby galaxies. Thermal noise is also added, based on the science requirements of KSG 3 (NGA8). The simulations used one channel with a center frequency of 115 GHz as a proxy for a single channel of a spectral line cube. `simobserve` alters the original frequency of the observations to the desired one in this case, changing the frequency of the PHANGS image from 230 GHz to 115 GHz. Additionally, the model has been scaled to a representative value of the expected peak flux of the line emission in a (2 km/s channel), in this case in `simobserve` we set

[9] The Physics at High Angular resolution in Nearby GalaxieS (PHANGS) using the Atacama Large Millimeter/Submillimeter Array (co-PI: A. Leroy)

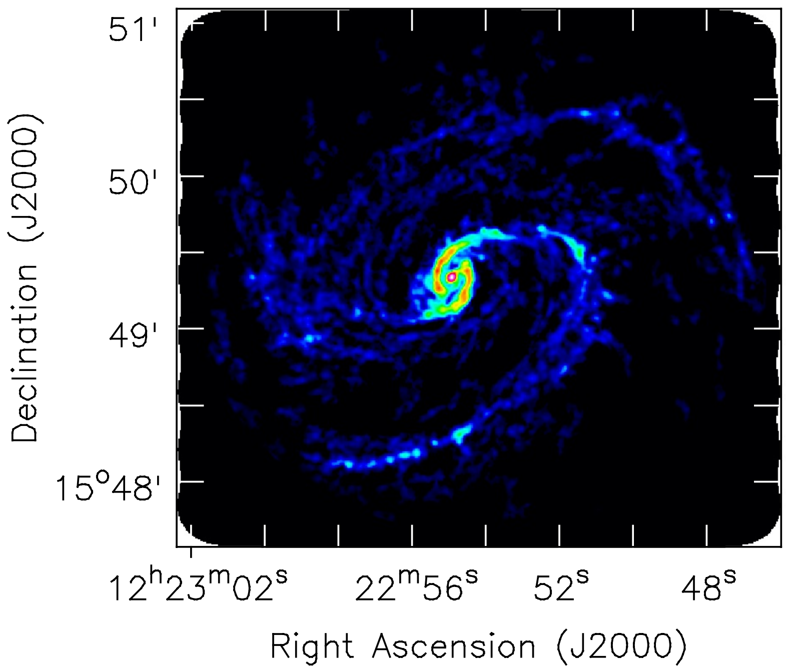


Figure 26: Image of NGC 4321 from the PHANGS-ALMA survey used for making the model image for our study.

`nbright`="0.019Jy/pixel". This value is estimated from scaling an image of M31 to the distance of Virgo to approximate a typical spiral galaxy for this KSG.

- ***Spiral+Core***: visibilities generated with CASA task `simobserve` using a 3.9 hr synthesis centered on transit[10]. We used a mosaic of 67 pointings (fields) and an integration time of 10 s[11], which corresponds to 21 scans/field.
- ***SBA***: visibilities generated with CASA task `simobserve` using a 8.6 hr[12] synthesis centered on transit. We used a mosaic of 7 pointings (fields) and an integration time of 10 s, which corresponds to 442 scans/fields.
- ***Total Power***: In this case, we directly made the simulated image by

[10]The actual observations would need to be longer to meet the target sensitivity. We selected 3.9 hrs to simplify the simulations, e.g., to avoid a simulation that spans multiple days. The amount of noise is scaled such that the final image will have the target sensitivity.

[11]This is the default value in `simobserve` that we choose for convenience to keep the measurement set files small. Time smearing is not an issue for simulated observations, but this value would need to be reconsidered before scheduling actual observations.

[12]This is equivalent to an integration time ratio $t_{sba}/t_{core} = 2.2$ which was used in ngVLA memo #67 [12].

running the CASA task `imsmooth` on the model image. The resolution of the simulated image is 38.64 arcsecs, which is close to the expected primary beam size of one of the 18m total power antennas (and takes into account other parameters such as blockage diameter, etc).

In order to concatenate the Spiral+Core with the SBA measurement sets we run the `concat` task and scale the relative weights based on the diameter of the dishes, thus reflecting the sensitivity of the visibilities.

### 3.2.2 Imaging

The imaging was done using the CASA task `tclean` on the MS produced by `concat` (i.e., the concatenation of the Plains+Core and the SBA datasets). The input model was spatially correlated on scales of $1.7''$ [13] and so the resulting image at 100 mas resolution will have a high degree of smoothness. Due to the amount of extended emission, cleaning required a very large number of minor cycle iterations in order that the residuals approached the thermal noise level ($>$ 500,000 iterations).
The imaging parameters that we used are the following:

- `multiscale` imaging with a range of scales to improve the speed and quality of the deconvolution (which also helps with the smoothness of the input model)
- `robust=0` together with a `taper=83.85` mas; combination that yields a beam of 100 mas, a PSF level 14% and a loss in sensitivity of $\sim 1.6$
- Interactive masking; to adjust the mask each major cycle, largely to avoid cleaning negative regions created by PSF sidelobes
- Image size of 12288 pixels; to achieve a field of view that includes the entire primary beam of the outer mosaic pointings, which minimizes aliasing
- Cell size of 20 mas; to oversample the restoring beam by a factor of 5

Then, the resulting mosaic is combined with the Total Power image using the CASA task `feather` (see ngVLA #89 [21] for more details in the procedure). The resulting image is shown in Figure 27.

### 3.2.3 Results

The final fidelity calculated using Equation 1 is 0.9898, representing the weighted average of the difference between the final image and the input model. Figure 28 shows an image of the fundamental term in the fidelity calculation prior to weighting and averaging, i.e., image minus model. The image area corresponds to the size of the cutout region. The residuals over most of the galaxy

[13] This scale corresponds to the pixel size of the PHANGS model; thus there is no detail on any smaller scales except for the added thermal noise.

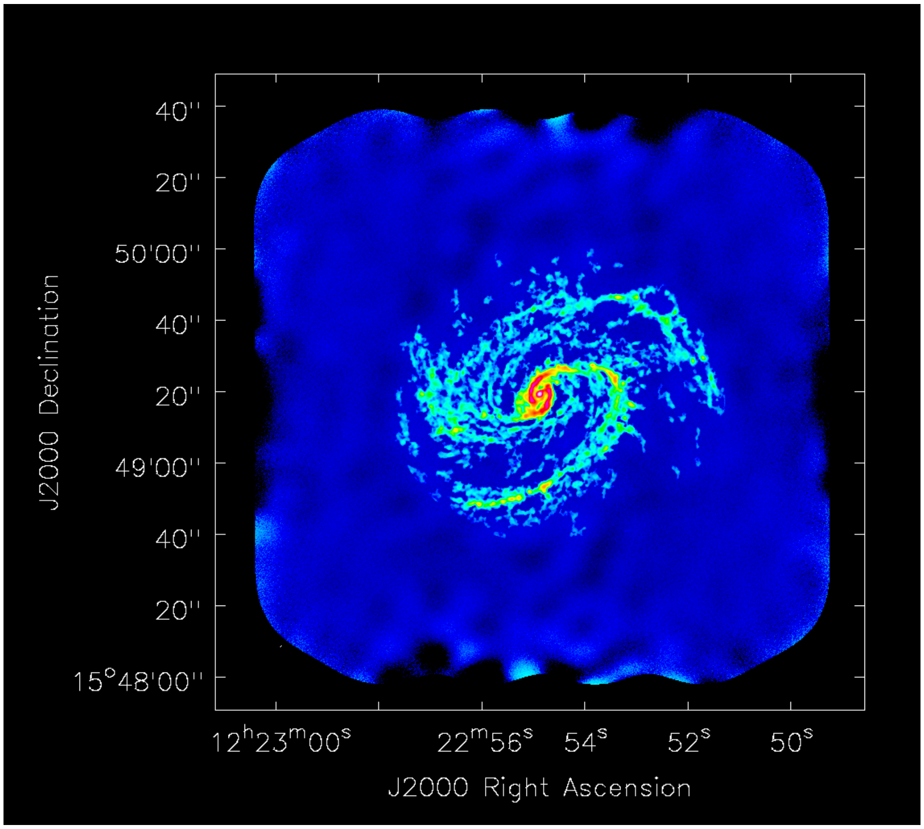


Figure 27: The final image after feathering.

are characteristic of the residuals created by multi-scale clean, and are of the same order of magnitude as the thermal noise. Larger magnitude residuals are present at the position of the galaxy's core and the bright, inner portions of the spiral arms. At these locations the intensity of the final image is $\lesssim 1\%$ higher than that of the convolved model, so while the absolute error causes these regions to stand out, the relative error does not seem unusual. Figure 29 shows an image of the fundamental term in the fidelity calculation prior to weighting and averaging, i.e., image minus model divided by model. You can think about this image as the fidelity per pixel. The unmasked pixels in Figure 29 have a standard deviation of 0.032 and a median value of $-0.01$.

Figure 30 shows the accuracy with which flux is recovered as a function of angular scale in each simulated image (see ngVLA memo #67 [12] for more details about the used heuristic), and calculating the median fraction of integrated flux recovered in a circular aperture compared to the simulation input image as a function of aperture radius. The final image after feathering using all the

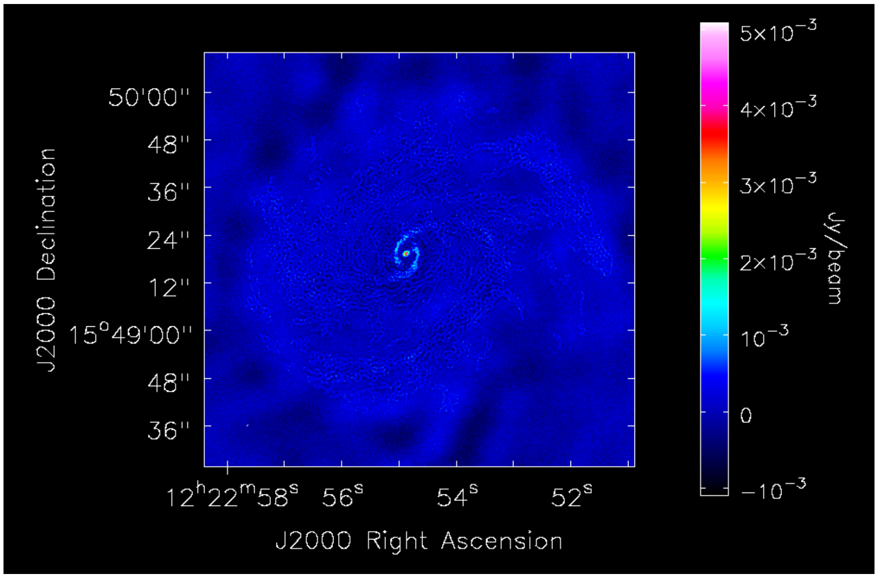


Figure 28: Image of the convolved model subtracted from the final image.

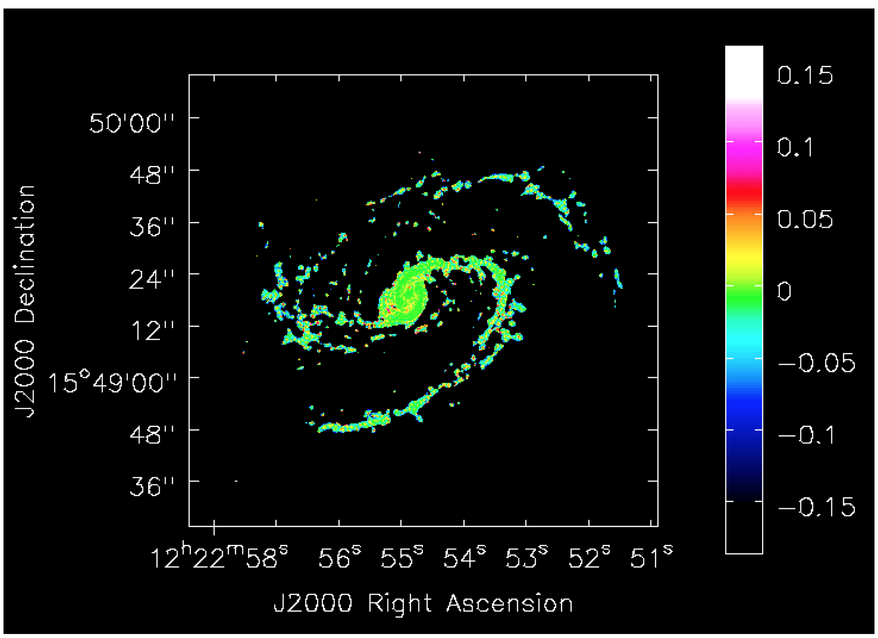


Figure 29: Image of the relative residuals, i.e., (model-image)/model. The image is masked where the convolved model is fainter that 5 mJy/beam.

considered arrays recover the input flux to better than 5% at all scales.

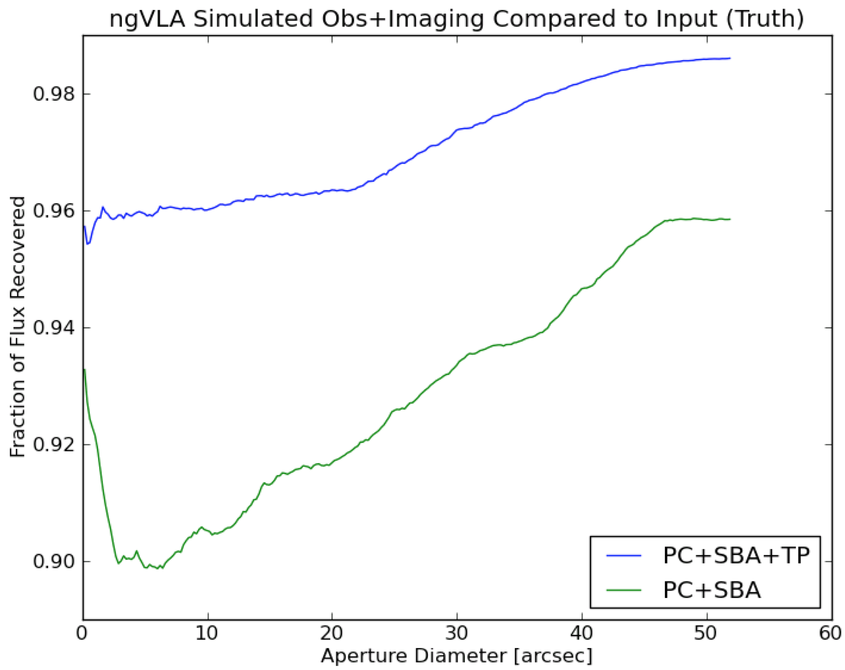


Figure 30: Median fraction of spatially integrated flux density recovered as a function of aperture diameter for the image made from the concatenated data set (Plains+Core plus SBA) and from the same image after feathering with total power.

#### 3.2.4 Comparison Study of image Fidelity using ngVLA RevC and RevD

The addendum of ngVLA memo #89 [21] presents a systematic comparison study of the RevC and RevD array configurations for the image fidelity using the same model from above. For this comparison, we adopt the auto-multithresh option that implements an automated masking algorithm (instead of the careful interactive masking used in the results presented before). We also choose a common threshold of 1 mJy and 500,000 iterations to ensure that this limit is reached, which allows us to clean down to the same peak residual and perform a more direct comparison between the images obtained from the RevC and RevD configurations. Using ngVLA mock observations of an NGC 4321 galaxy, we find that both the RevD and RevC configurations lead to an imaging fidelity of $\approx 0.994$.

# 4 High Dynamic Range Imaging

ngVLA memo #64 [8] explores the capability of the ngVLA to produce a high dynamic range, high fidelity image of an extended source with complex morphology. This requirement is delineated in:

- **SCI0108**: The ngVLA should produce high fidelity imaging ($> 90\%$) over a wide range of scales, spanning from a few arcmin to a few mas.
- **SCI0113**: The system brightness dynamic range shall be better than 50 dB to support deep field studies at 10 GHz.

We consider two definitions of image fidelity. The first is the ALMA usage, as given in Equation 1. The second is defined as:

$$F = (Data - Model)/Model$$

In this definition, a 90% value as employed in SCI0108, corresponds to a fidelity factor, $F < 10\%$, in absolute value.
While SCI0113 is designed more for continuum deep fields, the desire to obtain 50 dB dynamic range on complex extended objects is implicit in numerous science programs being envisioned in the Design Reference Science Mission.

## 4.1 Model, Configuration, and Processing

The input model we employ is a high dynamic range image of Cygnus A made with the VLA at 8 GHz. In the original image, the resolution is 0.35", and the source maximum extent is $\sim 2'$. The total flux density of Cygnus A at 8 GHz is 241 Jy.
We then modified the model to obtain a smaller source at higher resolution, by adjusting the pixel scale down. This scaling leads to an input model resolution of 0.1", and source maximum size of 40".
The input model image was then blanked in a few ways. First, all negative pixels were set to zero, since the true continuum sky has no 'negative emission'. Second, a fairly tight window was set around the radio lobes and jets, and zeroed outside the window. Lastly, the compact radio core source was blanked in the initial input model, then re-added as a point source model in the final image.
Choosing a real source for the model image is useful in terms of having astrophysically relevant quantities as the target. However, such a choice leads to two limitations. First, the input model itself has a dynamic range of only a few $\times 10^4$. Through the blanking process, we have removed the noise in regions off the radio source. Still, there are residuals within the radio lobes that are not real structure. In this case, the goal becomes to reproduce the model surface brightness, both real and noise. And second, the input model has an intrinsic resolution of 0.1", comparable to the target resolution of the simulation. In essence, the sky has been 'pre-convolved' before imaging (besides the core, which was set to be a point source). Most of the radio lobe structure appears

to be well resolved at this resolution, as seen on the highest resolution images made at 43 GHz with the VLA (Carilli et al. 1999 [10]), except perhaps the sharpest features in the radio hot spots.
Hence, the goal is not to obtain a better image of the source than the input model (that would be impossible). The goal is to reproduce the input model as best as possible, errors and all.
We employ a single channel of 50 MHz at 8.0 GHz to set the noise per visibility, and a 6 hour synthesis. This channel width would be adequate to avoid significant bandwidth smearing on scales relevant to the model source. The theoretical noise is then 0.62 uJy beam$^{-1}$ (ngVLA ETC).
For the configuration, we use the RevD Main array (ngVLA memo # 92 [9]). We run `SIMOBSERVE` for a six hour synthesis, with 30s records. We target a resolution comparable to the HST, or 0.12". The time resolution would be adequate to mitigate temporal smearing on the relevant scales of the source[14]. We then add noise to each visibility at the level appropriate for the record length and channel width.
We explored numerous CLEAN options. We found a multiscale clean was necessary, and that Uniform weighting with a Gaussian taper was preferred to reach the nominal specifications of $\sim 0.1$" resolution and a 50 dB dynamic range. The following CLEAN inputs were employed: Uniform weighting, cell size of 0.02", outer taper = 0.12", multiscale = [0,7,25], clean threshold of 0.2 mJy. A tight box was set around the radio source for CLEANing.

## 4.2 Results

The final CLEAN image is shown in Figure 31. This image has an off-source rms noise of 26 $\mu$Jy beam$^{-1}$, a peak surface brightness of 2.8 Jy beam$^{-1}$ (on the southern hot spot), and a beam FWHM = 0.129" $\times$ 0.122". Hence, the dynamic range (peak/rms), is $\sim 1.1 \times 10^5$. The total flux density in both the input model, and the CLEANed image, is 241 Jy. The radio core in both cases is 1 Jy.
Figure 31a shows a saturated version of the CLEAN image to emphasize the noise characteristics. Very low level sidelobes can be seen emanating primarily from the hot spot regions, indicating that the image is dynamic range limited. Again, the NA weighted theoretical noise is a factor 40 below the measured rms. We then created a fidelity image, $F$, by convolving the model with the CLEAN beam, and calculating the $F$ factor as defined above. The fidelity image is shown in Figure 32. In the division process, we blank the model image at 10 times the rms noise, to avoid taking ratios in regions where noise itself will limit fidelity to $< 0.9$, and to avoid division by zero.

Across the brighter parts of the lobes and hot spots, the fidelity has an rms of 0.46% in the brighter regions of the lobes, 0.9% in the tails, increasing to 4% in

[14] Neither time smearing or bandwidth smearing will occur using SIMOBSERVE since the calculations of geometry per visibility assume discrete values of time and frequency.

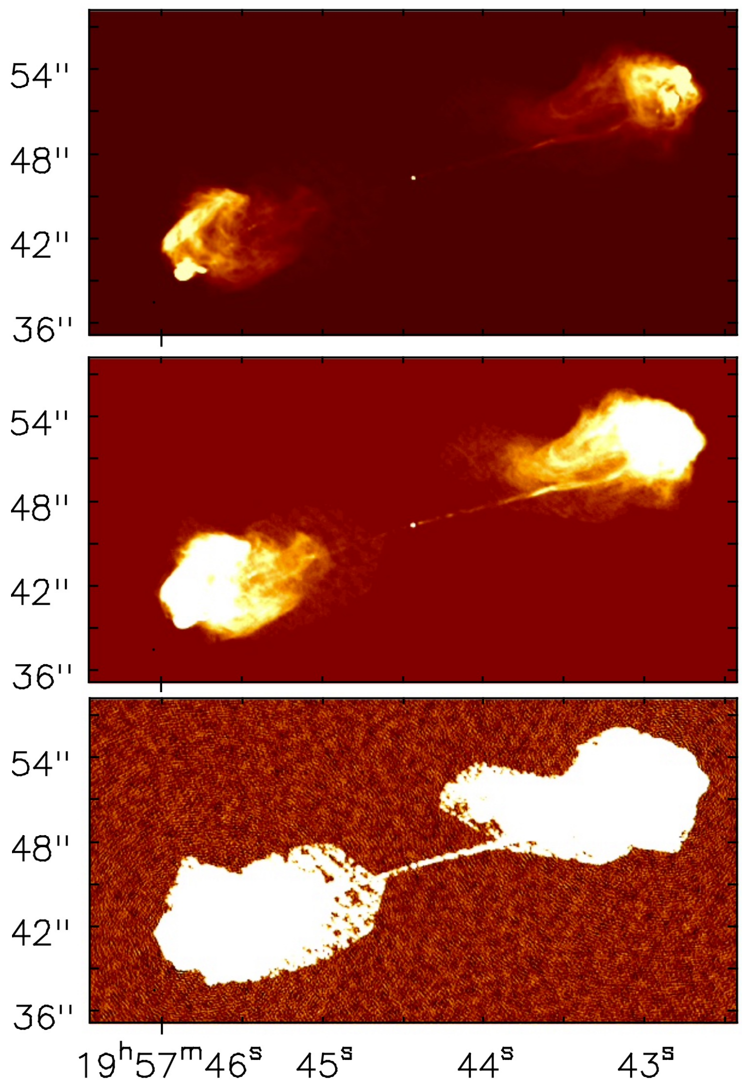


Figure 31: Simulated images of the Cygnus A scaled model for the ngVLA Main array tapered to 0.12" resolution. Three color scales are shown, emphasizing bright and faint emission, and the noise.

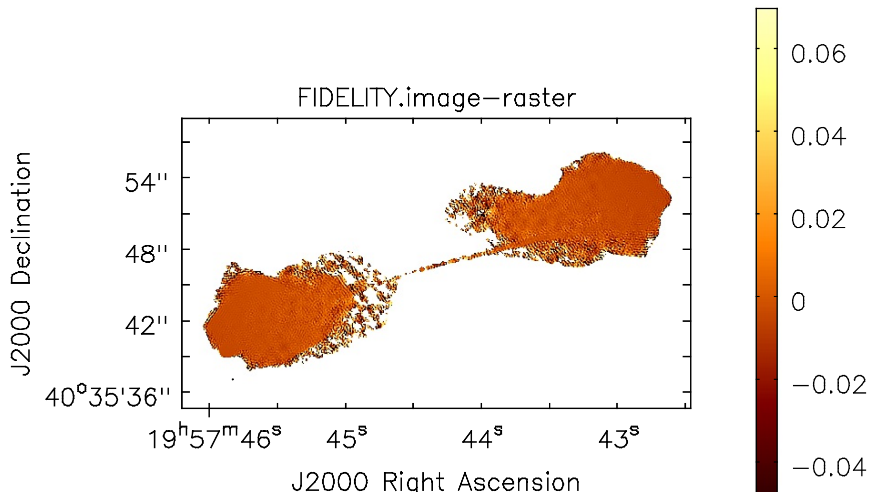


Figure 32: Fidelity image of Cygnus A as defined in Section 32. The image has been blanked at $10\sigma$ surface brightness on the input model.

the faintest regions of the source. There is no tendency for a bias, and we easily reach the $F < 10\%$ fidelity target across the source, in both the bright hot spot regions and across the fainter radio lobes of Cygnus A.

For comparison, the final fidelity calculated using Equation 1 is 99.5%, representing the weighted average of the difference between the final image and the input model. Figure 33 shows the PSF for this simulation. The peak negative sidelobes are -5.4%, and the PSF drops to $\sim$ 10% at a radius of $\sim$ 0.12".

## 4.3 Summary

We have performed high dynamic range imaging simulations of a complex extended object at 8 GHz. Even for a monochromatic simulation, the ngVLA main array was able to reach a dynamic range of $\sim 1.1 \times 10^5$ at a resolution of 0.12".

The rms image fidelity, $F_{rms} \sim 0.46\%$ in the brighter regions, and even in the faintest parts of the lobes, the rms fidelity remains high: $F_{rms} \sim 4\%$. There is no positive or negative bias of the data relative to the model.

The next step in the simulations process will be to incorporate multifrequency synthesis. The imaging and deconvolution process then becomes computing intensive, when including both MFS and a multiscale clean.

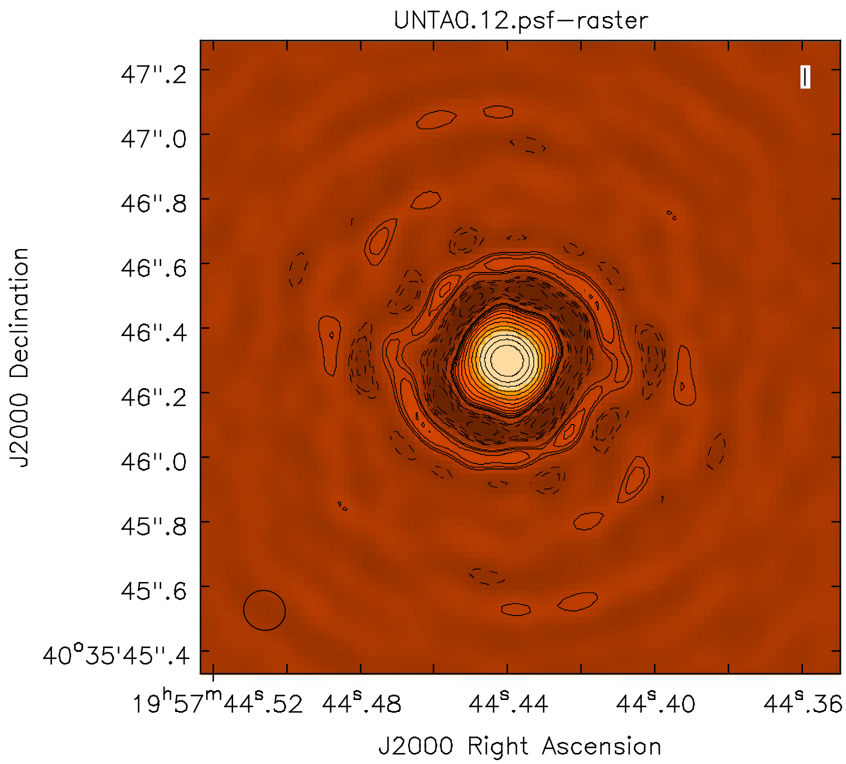


Figure 33: Images of the synthesized beam. Contour levels are a geometric progression in square root two starting at 1%, such that each two levels is a factor two increase in surface brightness. Negative contours levels are dashed.

# 5 On the Fly Mapping

We briefly consider the capabilities of the ngVLA for on-the-fly mapping. This is a multi-dimensional problem, with survey requirements that include area, depth, and total time available. For illustrative purposes, we make a very simple comparison to the parameters as used for the VLA Sky Survey (VLASS), and ignore issues such as overhead.

For the VLASS, the frequency range was 2 GHz to 4 GHz, with a scan speed of $3.3'$ sec$^{-1}$. The primary beam of the VLA $FWHM = 0.23^o = 14'$. The rows for the VLASS are separated by the $HWHM \sim 7'$, to provide roughly uniform sensitivity over the area. The time to cross the $FWHM$ of the primary beam at the scan rate is $\sim 4$ seconds, which is approximately the effective integration time for each position in the field[15]. The expected rms is 120$\mu$Jy beam$^{-1}$ per epoch of the VLASS.

As an example, assume a survey area of $10^o \times 5^o$. To scan over $10^o$ at $3.3^o$ min$^{-1}$ will take 3min. To cover $5^o$ in a series of rows separated by the $HWHM/2 = 0.12^o$ requires 42 rows. Hence, the total time required is 126 minutes.

Next, consider the ngVLA main array at 3 GHz with a 2 GHz bandwidth. To simplify this multidimensional problem, we fix the total area covered, and the total integration time, and determine the sensitivity. The primary beam $FWHM = 19' = 0.32^o$. Hence, 31 rows are required to cover $5^o$ at the $HWHM$ spacing. Assuming a total integration time of 126 min then leads to $\sim 4$ min per row, or a scan rate of $2.5^o$ min$^{-1}$. The crossing time of the primary beam $FWHM$ is then 7.7 sec, which, again corresponds roughly to the effective integration time per position. According to the latest ngVLA sensitivity calculator, the naturally weighted sensitivity of the ngVLA at 3 GHz is 0.24 $\mu$Jy hour$^{-1}$, so in 7.7 sec the sensitivity would be $\sim 5.2$ $\mu$Jy beam$^{-1}$. However, obtaining a reasonable synthesized beam shape through visibility weighting will increase the noise by roughly a factor 1.5 to 2, for target resolutions ranging from 0.1" to 5" at 3 GHz (ngVLA memo #55 [17]). Hence, the expected noise for tapered images will be within 30% of $\sim 9$ $\mu$Jy beam$^{-1}$, over this broad resolution range.

In summary, for a fixed survey area and integration time, an ngVLA OTF survey would be about 13 times more sensitive than the current VLASS. The example above is not necessarily an optimal approach for an OTF survey by the ngVLA, just an illustration of the capabilities in a specific situation.

[15] The fall-off of the primary beam during transit is off-set by adding the contribution of the neighboring rows

## Acknowledgments

We thank Brian Mason for providing the ALMA fidelity calculations for Section 4. The National Radio Astronomy Observatory is a facility of the National Science Foundation operated under cooperative agreement by Associated Universities, Inc. This study made use of the CASA task `iring`, an open-source tool from the Nordic ALMA regional center.

## References

[1] Bolatto A., Chatterjee S., et. al., *Next Generation Very Large Array Memo No. 19 Key Science Goals For The Next Generation Very Large Array (Ngvla): Report From The Ngvla Science Advisory Council.*

[2] Butler B., et. al., *Next Generation Very Large Array Memo No. 21 ngVLA Sensitivity.*

[3] Carilli C., *Next Generation Very Large Array Memo No. 12 The Strength of the Core.*

[4] Carilli C., Shao Y., *Next Generation Very Large Array Memo No. 13 Imaging Capabilities: High Redshift CO.*

[5] Carilli C., *Next Generation Very Large Array Memo No. 16 More on Synthesized Beams and Sensitivity.*

[6] Carilli C., Erickson E., *Next Generation VLA Memo. 41 Initial Imaging Tests of the Spiral Configuration.*

[7] Carilli C., *Next Generation Very Large Array Memo No. 47 Resolution and Sensitivity of ngvla-revB.*

[8] Carilli C., *Next Generation Very Large Array Memo No. 64 High Dynamic Range Imaging.*

[9] Carilli C., et. al., *Next Generation Very Large Array Memo No. 92 Configuration: Reference Design Rev D Description.*

[10] Carilli, C., et al. 1999, AJ, 118, 2581

[11] Clark B., Brisken W., *Next Generation Very Large Array Memo No. 3 Possible Configurations for the ngVLA.*

[12] Mason, B., *Next Generation Very Large Array Memo No. 67 Demonstration & Analysis of ngVLA core + Short Baseline Array Extended Structure Imaging.*

[13] Murphy E., Selina R., ngVLA SAC, *ngVLA Science Requirements document 020.10.15.05.00–0001–REQ.*

[14] Ricci L., et. al., *Next Generation Very Large Array Memo No. 33 Investigating The Early Evolution Of Planetary Systems With Alma And The Next Generation Very Large Array.*

[15] Ricci, L., Isella, A., Liu, S., & Li, H. 2018, in Astronomical Society of the Pacific Conference Series, Vol. 517, Science with a Next Generation Very Large Array, ed. E. Murphy, 147

[16] Ricci, L., Liu, S.-F., Isella, A., & Li, H. 2018b, ApJ, 853, 110

[17] Rosero, V., *Next Generation Very Large Array Memo No. 55 Taperability Study for the ngVLA and Performance Estimates.*

[18] Rosero, V., *Next Generation Very Large Array Memo No. 65 Sculpting of the Synthesized Beam and Image Fidelity Study of KSG 1: Imaging of Protoplanetary Disks.*

[19] Rosero, V., *Next Generation Very Large Array Memo No. 72 A Study of ngVLA Subarray Efficiency: Plains + Fractions of the Core.*

[20] Rosero, V., *Next Generation Very Large Array Memo No. 76 Subarray Selection for the Reference Observing Program.*

[21] Rosero, V., *Next Generation Very Large Array Memo No. 89 Image Fidelity Study of KSG 3 (NGA8): Imaging Molecular Gas in Nearby Galaxies.*

[22] Woody, D., *ALMA Memo No. 389 Radio Interferometer Array Point Spread Functions. I. Theory and Statistics*